Fisheries and Oceans Canada | Pêches et Océans Canada
Ecosystems and Oceans Science | Sciences des écosystèmes et des océans

Canadian Science Advisory Secretariat (CSAS)

Research Document 2019/009

Québec Region

Chemical and Biological Oceanographic Conditions in the Estuary and Gulf of St. Lawrence during 2017

M. Blais, P. S. Galbraith, S. Plourde, M. Scarratt, L. Devine and C. Lehoux

Fisheries and Oceans Canada
Institut Maurice-Lamontagne
850 route de la Mer, P.O. Box 1000
Mont-Joli, QC, G5H 3Z4

June 2019

Canada

Foreword

This series documents the scientific basis for the evaluation of aquatic resources and ecosystems in Canada. As such, it addresses the issues of the day in the time frames required and the documents it contains are not intended as definitive statements on the subjects addressed but rather as progress reports on ongoing investigations.

Published by:

Fisheries and Oceans Canada
Canadian Science Advisory Secretariat
200 Kent Street
Ottawa ON K1A 0E6

http://www.dfo-mpo.gc.ca/csas-sccs/
csas-sccs@dfo-mpo.gc.ca

ISSN 1919-5044

Correct citation for this publication:

Blais, M., Galbraith, P.S., Plourde, S., Scarratt, M., Devine, L. and Lehoux, C. 2019. Chemical and Biological Oceanographic Conditions in the Estuary and Gulf of St. Lawrence during 2017. DFO Can. Sci. Advis. Sec. Res. Doc. 2019/009. iv + 56 pp.

Aussi disponible en français :

Blais, M., Galbraith, P.S., Plourde, S., Scarratt, M., Devine, L. et Lehoux, C. 2019. Les conditions océanographiques chimiques et biologiques dans l'estuaire et le golfe du Saint-Laurent en 2017. Secr. can. de consult. sci. du MPO. Doc. de rech. 2019/009. iv + 59 p.

TABLE OF CONTENTS

ABSTRACT

An overview of chemical and biological oceanographic conditions in the Gulf of St. Lawrence (GSL) in 2017 is presented as part of the Atlantic Zone Monitoring Program (AZMP). AZMP data as well as data from regional monitoring programs are analyzed and presented in relation to long-term means in the context of a strong warming event that began in 2010. Oxygen levels at 300 m reached their lowest concentration measured so far in several GSL regions during 2017. Negative anomalies in deep O_2 concentration were especially strong in central GSL and the Cabot Strait region. Nitrate inventories in the surface layer (0–50 m) were generally near normal everywhere in the GSL all year round. However, they were above normal in deep waters of eastern GSL (eGSL), which has been observed since 2012 and is associated with intrusions of warm and salty waters. Vertically integrated chlorophyll *a* (chl *a;* 0–100 m) was below normal in western GSL (wGSL) and above normal in southern GSL (sGSL) during summer and fall. In sGSL, the positive chl *a* anomaly measured *in situ* was actually the strongest recorded since 2002. However, according to satellite imagery, the spring bloom amplitude was generally below normal everywhere in the GSL, including sGSL. Satellite estimates show a near-normal surface chl *a* annual mean throughout the GSL despite low spring biomass. Dinoflagellate abundance reached a record low at Rimouski station, while it was above normal at Shediac Valley as were flagellates and ciliates at this station. In 2017, zooplankton biomass was below average everywhere in the GSL, but the main zooplankton functional groups and species abundances were all above normal in eGSL with the exception of *Calanus hyperboreus*. In wGSL and sGSL, *C. finmarchicus*, *Pseudocalanus* spp., and total copepod abundances showed negative anomalies. It is the first time since 2012–2013 that negative anomalies have been recorded for *Pseudocalanus* spp. Moreover, the widespread positive anomalies of small calanoid abundance that have been observed since 2008 were restricted to Rimouski station and eGSL in 2017. Higher-than-normal abundances of copepod species associated with warm water were again observed in 2017, continuing a trend observed since 2011. Development of *C. finmarchicus* was delayed at Rimouski station in 2017, unlike observations in recent years. Some of these phytoplankton and zooplankton dynamics could reflect the influence of a St. Lawrence freshwater runoff well above the normal in May and June 2017 and of year-round warmer-than-normal deep waters.

INTRODUCTION

The Atlantic Zone Monitoring Program (AZMP) was implemented in 1998 (Therriault et al. 1998) with the aim of (1) increasing Fisheries and Oceans Canada's (DFO) capacity to understand, describe, and forecast the state of the marine ecosystem and (2) quantifying the changes in the ocean's physical, chemical, and biological properties and the predator–prey relationships of marine resources. AZMP provides data to support the sound development of ocean activities. A critical element in the observational program of AZMP is an annual assessment of the distribution and variability of nutrients and the plankton communities they support.

A description of the spatiotemporal distribution of dissolved oxygen, nutrients (nitrate, silicate, phosphate), and chlorophyll *a* concentrations provides important information on water-mass movements and on the locations, timing, and magnitude of biological production cycles. A description of phytoplankton and zooplankton distribution provides important information on the organisms forming the base of the marine food web. An understanding of plankton production cycles is an essential part of an ecosystem approach to fisheries management.

The AZMP derives its information on the state of the marine ecosystem from data collected at a network of sampling locations (high-frequency monitoring sites, cross-shelf sections) in each DFO region (Québec, Gulf, Maritimes, Newfoundland; see Figure 1 for Québec region locations) sampled at a frequency of weekly to once annually. The sampling design provides valuable information on the natural variability in physical, chemical, and biological properties of the Northwest Atlantic continental shelf: cross-shelf sections provide detailed geographic information but are limited in their seasonal coverage while critically placed high-frequency monitoring sites complement the sampling by providing more detailed information on annual scale changes in ecosystem properties.

In this document, we review the chemical and biological oceanographic (lower trophic levels) conditions in the Gulf of St. Lawrence (GSL) in 2017. Oceanographic physical conditions that prevailed in 2017 are described in Galbraith et al. (2018). Overall, temperature conditions were warmer than normal during the whole year, the maximum volume of sea-ice cover was the sixth lowest since 1969, and the onsets of summer warming and fall cooling were respectively slightly earlier and later than normal. The annual average freshwater discharge into the Estuary was the highest since 1974. Deep-water temperatures were again above normal with inward advection from Cabot Strait. GSL average temperature reached a record high at 300 m. This report describes the 2017 production cycles and community composition of phytoplankton and zooplankton in this context.

METHODS

SAMPLE COLLECTION

All sample collection and processing steps meet and often exceed the standards of the AZMP protocol (Mitchell et al. 2002). Field measurements included in this report were made along seven sections during surveys carried out in winter, summer, and fall (usually in March, June, and November) of each year and at two high-frequency monitoring sites (Fig. 1). In this document, the seven sections were grouped into three subregions to better correspond to the spatial scales addressed by AZMP in other regions:

(1) western GSL (wGSL): this region is generally deep (> 200 m) and cold in summer. It is strongly influenced by freshwater runoff from the St. Lawrence River and cold and dense waters from the Laurentian Channel. It includes TESL, TSI, and TASO sections;

(2) southern GSL (sGSL): this region is shallow (< 100 m) and much warmer in summer. It is under the influence of the Gaspé Current and includes TIDM section only;

(3) eastern GSL (eGSL): this region, with deep channels and a relatively wide shelf (< 100 m), is characterized by higher surface salinity and is directly influenced by the intrusion of water from the Labrador and Newfoundland shelves. It includes TCEN, TDC, and TBB sections.

Table 1 provides details about the 2017 sampling surveys and Figure 2 summarizes the sampling effort at the high-frequency sampling sites. Rimouski station (depth 320 m) has been sampled since 1991 as part of a research project—about weekly throughout the summer, less frequently in early spring and late fall, and rarely in winter (except during the winter survey). It has been included in AZMP's annual review of environmental conditions since 2004 to represent conditions in the St. Lawrence Estuary (SLE) and the northwest GSL. Since the beginning of the AZMP, Shediac Valley station (depth 84 m) has represented conditions in the southern GSL and SLE outflow. While the goal is to sample Shediac Valley station twice a month, the frequency is closer to monthly and even less frequent during January–April because of its remoteness. Sampling at sections and high-frequency monitoring sites includes a CTD profile (temperature, salinity, fluorescence, dissolved oxygen) as well as water sampling using Niskin bottles. Water from the Niskin bottles is collected for the analysis of dissolved oxygen (Winkler method), nutrients (Technicon or Alpkem AutoAnalyzer), chlorophyll a (chl a), and phytoplankton identification (inverted microscopy) (Mitchell et al. 2002). Finally, mesozooplankton (< 1 cm) were sampled with bottom-to-surface ring net tows (75 cm diameter, 200 µm mesh) for identification and biomass measurements.

Since 1996, a survey of the winter surface mixed layer of the GSL has been conducted, usually in early to mid-March, using a Canadian Coast Guard (CCG) helicopter. Surface nutrients (2 m) have been sampled since 2001 (Galbraith 2006, Galbraith et al. 2006), and additional depths were sampled in March 2016 and 2017 because sampling was carried out from CCG ships rather than the helicopter. This survey has added a considerable amount of data to the previously sparse winter sampling in the region. Forty-two stations were sampled between 1 and 12 March 2017.

OXYGEN

Oxygen concentration at 300 m are used as a monitoring indicator of hypoxic conditions in the GSL since it is less variable over time than surface oxygen concentrations, which vary seasonally because of water column mixing and primary production. Oxygen concentration was measured using an oxygen probe (Sea-Bird SBE43) mounted on the CTD; the probe was calibrated against seawater samples collected and analyzed by Winkler titration on every cast (for calibration procedure, see Sea-Bird application notes 61-1, -2, -3). We present here the mean annual concentrations of deep oxygen in the GSL derived from the CTD probe along with time series of annual concentrations of deep oxygen.

NUTRIENTS AND CHLOROPHYLL A

Chlorophyll a and nutrient data collected along the AZMP sections and the high-frequency monitoring sites were integrated over various depth intervals (i.e., 0–100 m for chl a; 0–50 m and 50–150 m for nutrients) using trapezoidal numerical integration. The upper integration limit was actually the shallowest sampled value, and the closest sampled depth to the lower integration limit was used in the calculation. In previous reports, integrated nitrate values from the winter survey were calculated using surface concentrations (2 m) × 50 m; it was assumed that nitrate concentrations are homogeneous in the winter mixed layer at that time of the year. In 2016 and 2017, the vertical profiles of nutrients at Rimouski station revealed that nitrate

concentrations were indeed relatively homogeneous in the upper 50 m of the water column during winter (around 14 mmol m^{-3}; see Results) The nutrient inventory in the upper (0–50 m) water column was also relatively homogeneous elsewhere in the GSL during the winter 2016 and 2017 surveys (data not shown), confirming the initial assumption.

In this document, a detailed description of the seasonal patterns is provided for different nutrient and phytoplankton indices. For the high-frequency monitoring sites, we present nitrate inventories in different water column layers, chl *a* concentration, phytoplankton abundance, and the relative abundance of the main phytoplankton taxonomic groups. For the three GSL subregions described above, the seasonal nitrate and chl *a* concentrations integrated over different depth layers as well as the spatial distribution of nutrients (nitrate, phosphate, silicate, N:P ratio) and chl *a* are presented. Spring nutrient drawdown was estimated using the difference in nitrate inventory between March and June. Anomalies were computed for these indices (see Scorecard section below) for both high-frequency monitoring sites and GSL subregions.

SATELLITE REMOTE SENSING OF OCEAN COLOUR

Satellite ocean colour data provide large-scale images of surface phytoplankton biomass (chl *a*) over the whole northwest Atlantic. We used two-week satellite composite images of four GSL subregions (northwest and northeast GSL [NWGSL, NEGSL], Magdalen Shallows, Cabot Strait; see Fig. 3 for locations) to supplement our ship-based observations, especially regarding spring bloom phenology, and to provide seasonal coverage and a large-scale context over which to interpret our survey data. The ocean colour imagery provides information about the timing and spatial extent of the spring and fall blooms but does not provide information on the dynamics that take place below the top few metres of the water column. In addition, satellite ocean colour data for the St. Lawrence Estuary are largely contaminated by suspended inorganic particulates and coloured dissolved organic matter that render these data too uncertain to be used in an absolute manner. While knowledge of phytoplankton dynamics at the surface of the St. Lawrence Estuary during spring is gathered using the weekly sampling at Rimouski station, the temporal resolution is not always good enough to allow the calculation of bloom metrics as discussed below. Thus, the spring bloom metrics are not presented for the Estuary but seasonal and interannual variability of phytoplankton biomass is described. In addition, the broad-scale oceanographic surveys include a transect in the Estuary (TESL) and are used to provide a general estimate of phytoplankton concentrations during summer and fall in this region.

Near-surface phytoplankton biomass has been estimated from ocean colour data collected by the Sea-viewing Wide Field-of-view Sensor (SeaWiFS) satellite launched by NASA in late summer 1997, by the Moderate Resolution Imaging Spectroradiometer (MODIS) “Aqua” sensor launched by NASA in July 2002, and most recently by the Visible Infrared Imaging Radiometer Suite (VIIRS) satellite, which was launched in October 2011. In this report, VIIRS data for the 2012–2017 period and MODIS data for the 2008–2011 period are combined with SeaWiFS data from September 1997 until December 2007 to construct composite time series of surface chl *a* in four GSL subregions (Fig. 3). The performance of the MODIS satellite to estimate chl *a* has been compared with that of SeaWiFS for some regions of the globe. Although differences in sensor design, orbit, and sampling between MODIS and SeaWiFS cause some differences in calculated chl *a* values (Gregg and Rousseaux 2014), the biases associated with these satellites are overall not significantly greater than algorithm uncertainties, particularly in non-turbid waters (Zibordi et al. 2006, Arun Kumar et al. 2015). Recent studies comparing all three sensors indicate that they provide consistent global ocean colour data records, with similar patterns and magnitudes and generally high cross-sensor fidelity, reflecting the strong performance of these sensors (Wang et al. 2013, Barnes and Hu 2016).

All selected subregions for the imagery data are located outside of the St. Lawrence River plume because data in regions influenced by this freshwater are unreliable as a result of turbidity and riverine input of terrestrially derived coloured matter, as mentioned previously. Composite satellite images were provided by BIO's remote sensing unit (Bedford Institute of Oceanography, DFO, Dartmouth, NS) in collaboration with NASA's Goddard Space Flight Center. Basic statistics (mean, range, standard deviation) were extracted from two-week average composites by averaging all pixels within each statistical subregion (SeaWiFS and MODIS have a 1.5 km spatial resolution while VIIRS has a 1 km spatial resolution).

A shifted Gaussian function of time model was used to describe characteristics of the spring phytoplankton bloom based on the combined satellite data (Zhai et al. 2011). Four different metrics were computed to describe the spring bloom characteristics: start date (day of year), cycle duration (days), magnitude (the integral of chl *a* concentration under the Gaussian curve), and amplitude (maximum chl *a*). In addition, the mean chl *a* biomasses during spring (March to May), summer (June to August), and fall (September to November) as well as its annual average (March to November) were computed. For each of these eight metrics, we computed normalized annual anomalies (see Scorecard section below) to evaluate evidence of temporal trends among the different statistical subregions.

ZOOPLANKTON INDICES

We also provide a detailed description of the seasonal patterns for different zooplankton indices, mostly at Rimouski and Shediac Valley stations, but also for the three GSL subregions described above. In recent years, the number and type of zooplankton indices as well as the way they are reported have been rationalized with the aim of standardizing research documents among AZMP regions. For the high-frequency monitoring sites, we thus present total zooplankton biomass (dry weight), total copepod abundance, and the relative contributions of the copepod species making up 95% of the identified taxa by abundance. In addition, we include *Pseudocalanus* spp. (Rimouski station only) and *Calanus finmarchicus* abundances and stage composition. Because of its importance to the total zooplankton biomass in the GSL, a detailed description of *Calanus hyperboreus* has been added for Rimouski and Shediac Valley stations. We also present the spring and fall total zooplankton biomass and total abundance of *C. finmarchicus*, *C. hyperboreus,* and *Pseudocalanus* spp. for the three GSL subregions since they have distinct oceanographic regimes. Zooplankton indices were integrated using sampled depth in recent years or bottom depth prior to 2015.

Changes in zooplankton phenology were described using *C. finmarchicus* as an indicator. We used the time series at Rimouski station because adequate sampling and stage identification started there more than 20 years ago (1994). From 1994 to 2004, prior to the use of the AZMP standard 75 cm diameter, 200 µm mesh bottom-to-surface ring net tows (Mitchell et al. 2002), *C. finmarchicus* copepodite stage abundance was determined using samples collected with 333 µm (CIV–CVI) and 73 µm (CI–III) mesh nets that were analyzed for seven years of the time series (see Plourde et al. 2009 for details). In other years before 2004 for which 73 µm samples were not analyzed, the abundance of CI–III in the 333 µm samples was adjusted based on a comparison done with a similar net (S. Plourde, DFO, Mont-Joli, QC, unpublished data). The phenology of *C. finmarchicus* was described using the following steps: (1) stage abundance data (ind. m^{-2}) were normalized (x/x_{max}) within each year for CI–III, CIV, CV, and CVI (male and female) and (2) relative stage proportions were smoothed using a Loess algorithm.

Finally, we present several zooplankton indices that reflect either key copepod species, different functional groups with different roles in the ecosystem, or groups of species indicative of cold- or warm-water intrusions and/or local temperature conditions specific to the GSL. These indices are for *C. finmarchicus*, *Pseudocalanus* spp., total copepods (main component of

mesozooplankton in terms of biomass and abundance), non-copepods (larval stages of benthic invertebrates, many carnivores that feed on other zooplankton, and small particle-feeding taxa), large calanoids (dominated by *Calanus* spp. and *Metridia* spp.), small calanoids (depending of the region, this group can be dominated by species such as *Pseudocalanus* spp., *Acartia* spp., *Temora longicornis*, and *Microcalanus* spp.), cyclopoids (dominated by *Oithona* spp. and *Triconia* spp.; the latter is a poecilostomatoid that is included in this category because of its ecological characteristics), warm-water species (*Metridia lucens*, *Centropages* spp., *Paracalanus* spp., and *Clausocalanus* spp.), and cold/arctic species (*Calanus glacialis* and *Metridia longa*). Anomalies were computed for these groups (see Scorecard section below) for both high-frequency monitoring sites and GSL subregions.

SCORECARDS

Standardized anomalies of standard chemical and biological indices presented in scorecards were computed for the high-frequency monitoring sites and oceanographic regions. These anomalies are calculated as the difference between the variable's average for the season (i.e., chlorophyll and nutrient indices) or for the complete year (i.e., zooplankton indices) and the variable's average for the reference period (usually 1999–2015); this number is then divided by the reference period's standard deviation. Previous reports used the 1999–2010 reference period for biogeochemical parameters. Considering the non-stationary state of the Atlantic system, extending the climatology to include recent years changes the mean against which observations are compared and changes the time-series variance that is used to normalize annual means. This can shift the sign or magnitude of anomalies and, thus, anomaly patterns will not be consistent with past reports. While this issue must be kept in mind, the advantage of the extended reference period is to provide more relevant depictions of current system conditions and trends.

Anomalies are presented as scorecards with positive anomalies depicted as shades of red, negatives as blues, and neutral (± 0.5 SD) as white. A standard set of indices representing anomalies of nutrient concentrations, phytoplankton biomass and bloom dynamics, and the abundance of dominant copepod species and groups (*C. finmarchicus, Pseudocalanus* spp., total copepods, and total non-copepods) are produced for each AZMP region. To visualize northwest Atlantic shelf-scale patterns of environmental variation, a zonal scorecard including observations from all of the AZMP regions is presented in DFO (2018).

Annual anomalies of nutrient and phytoplankton indices at high-frequency stations are averages of monthly anomalies while they correspond to the average of summer and fall anomalies for the three subregions. Annual zooplankton index anomalies are based on the mean annual abundance estimate at each fixed station and as an overall average for each GSL subregion. These annual abundance estimates use general linear models (GLM) of the form

$\mathrm{Log}_{10}(Abundance+1) = \alpha + \beta_{YEAR} + \delta_{MONTH} + \varepsilon$ for the fixed stations and
$\mathrm{Log}_{10}(Abudance+1) = \alpha + \beta_{YEAR} + \delta_{STATION} + \gamma_{SEASON} + \varepsilon$ for the sections,

as in Pepin et al. (2013) and Johnson et al. (2016). *Abundance* is in units of ind/m^{-2}, α is the intercept, and ε is the error. The GLM is applied to the three subregions separately. For the fixed stations, β and δ are the categorical effects for year and month, respectively. For the sections, β, δ, *and* γ take into account the effect of year, station, and season, respectively. An estimate of the least-square mean based on type III sums of squares was used as the measure of the overall year effect. Results of the GLM analysis for high-frequency monitoring stations and GSL subregions are shown in Appendices 1 and 2, respectively. We log-transformed density values before computing zooplankton anomalies to compensate for the skewed

distribution of the observations. One was added to the *Abundance* term to include observations with a value of 0.

OBSERVATIONS

PHYSICAL ENVIRONMENT

The temperature and salinity of the 2017 water column are described in Galbraith et al. (2018) in detail. Stratification is one of the key parameters controlling primary production. For this reason, we present the upper water column stratification at the high-frequency monitoring stations (Fig. 4). Higher-than-normal stratification values are shown as blue anomalies in this figure because they are usually caused by lower salinity in the upper layer. Stratification was well above normal during springtime at Rimouski station, especially in May, when it was the highest anomaly recorded since 1996, but timing was similar to the 1999–2015 average. Stratification was also above normal at Shediac Valley station in June and July. The strong stratification was caused by the unusually large spring freshet and the accumulation of freshwater in the Estuary and elsewhere in the GSL (Galbraith et al. 2018).

DEEP OXYGEN

In the GSL, a dissolved oxygen value of 100 µM corresponds to approximately 30% saturation, below which the water is considered to be hypoxic. The lowest levels of dissolved oxygen (around 20% saturation in recent years) are found in the deep waters at the head of the Laurentian Channel in the Estuary (Fig. 5). Concentrations of dissolved oxygen have strongly decreased in the GSL in 2017 (Fig. 5), reaching the lowest observed values since 2000 in all regions but the northwest GSL (Fig. 6). The deep waters of the Estuary have consistently been hypoxic since 1984; dissolved oxygen decreased to 54 µM in 2017, corresponding to ca. 18% saturation (Fig. 6). In 2017, the strongest negative anomalies were recorded in central GSL and in Cabot Strait region (Figs. 5, 6).

NUTRIENTS AND PHYTOPLANKTON

Distributions of the primary dissolved inorganic nutrients (nitrate, silicate, phosphate) included in AZMP's observational program strongly co-vary in space and time (Brickman and Petrie 2003). For this reason and because the availability of nitrogen is most often associated with phytoplankton growth limitation in coastal waters of the GSL, emphasis in this document is given to variability in nitrate concentrations and inventories, even though the distribution of other nutrients is also briefly discussed. In this document, we use the term "nitrate" to refer to nitrate+nitrite (NO_3^-+NO_2^-).

High-frequency monitoring sites

The main highlights of 2017 in terms of nitrate inventories and phytoplankton biomass are well illustrated in Figure 7 for both high-frequency monitoring sites. At Rimouski station, nitrate concentrations were near normal the whole year but phytoplankton biomass stayed generally below normal with the exception of two short blooms, one in late June and the other in early September (Fig. 7a, c). The annual averages of nitrate and phytoplankton biomass concentrations were near normal, except that the deep nitrate inventory was below normal (Fig. 7e). At Shediac Valley station, sampling was sparse and almost nonexistent during winter and early spring (Fig. 7b, d), rendering the detection of seasonal patterns difficult. From May until November, the surface nitrate inventory was generally above normal while chl *a* concentration was near normal (Fig. 7b, d, e).

Detailed nitrate and chl *a* vertical profiles and vertical anomaly patterns are shown in Figures 8 and 9 for Rimouski and Shediac Valley stations, respectively. Nitrate consumption started in late May at Rimouski station and increased in June, concomitant with a strong positive phytoplankton biomass anomaly. Later replenishment of nutrients in the surface layer allowed the occurrence of a second bloom in late summer. In contrast to what has been seen in recent years, there was no pulse of phytoplankton biomass between these two bloom events. Vertical export during springtime, as estimated from the chl *a* concentration below 50 m, was also reduced in comparison with recent years (Fig. 8). There were a few strong positive nitrate anomalies in the surface layer at Shediac Valley station during summer. Interestingly, there was also a strong phytoplankton biomass accumulation near 40 m depth during May, which differs from previous years (Fig. 9).

Phytoplankton abundance at Rimouski station was slightly below normal most of the year and was dominated by flagellates except during the two short bloom events when diatoms were dominant (Fig. 10 a, c). Thus, the relative abundance of the main phytoplankton taxonomic groups in 2017 was very different from the typical seasonal pattern, where diatoms show a sharp increase in April and make up most of the phytoplankton abundance from May to October (Fig. 10b, c). The annual (May–Nov.) anomalies for diatom and flagellate abundances were near normal, but the large seasonal variability in phytoplankton abundance makes it difficult to detect anomaly patterns. Dinoflagellates showed the strongest negative anomaly of the time series, and negative anomalies for this taxon have been observed since 2013 at Rimouski station (Fig. 11). At Shediac Valley station, phytoplankton abundance showed wide variations above and below the long-term mean in spring, was near normal during summer and late fall, and above normal in November (Fig. 12a). Relative diatom abundance represented only about 10% of total phytoplankton abundance during summer 2017, whereas it typically remains stable at around 80% from spring to fall (Fig. 12b, c). Flagellates dominated phytoplankton abundance during summer 2017. Overall, flagellate, ciliate, and dinoflagellate abundances all showed positive annual anomalies in 2017 (Fig. 11). However, these seasonal patterns and annual anomalies must be interpreted carefully considering that only seven phytoplankton samples were analyzed at this station in 2017 and there was no sampling in April, when the spring diatom bloom usually occurs.

Gulf subregions

Overviews of the seasonal distribution of nutrient inventories, phytoplankton biomass, and their anomalies in the GSL are presented in Figures 13 to 17. Surface layer nitrate inventories were generally near normal most of the year throughout the GSL with negative anomalies in wGSL and eGSL during winter and summer, respectively. Negative anomalies of surface nitrate inventory have been observed regularly since 2010 in all GSL subregions, particularly during wintertime (Fig. 13). In the absence of sampling during the spring bloom, the spring nutrient drawdown estimated from the difference in nitrate inventory in the surface layer between the winter and the summer cruises is used to infer spring productivity. The distribution of spring nutrient drawdown shows a widespread negative anomaly in wGSL and around the Gaspé Peninsula (Fig. 14). Normal or slightly above-normal nitrate drawdown was observed elsewhere in the GSL (Figs. 13, 14).

Nitrate inventories were averaged for summer and fall over each subregion and over different water column layers (Fig. 13, middle panel) to serve as an indicator of the average annual nutrient pool available during the productive season. Positive anomalies for nitrate concentrations at 300 m were observed again this year in eGSL, where above-normal nitrate concentrations have been observed since 2012 (Fig. 13). The amounts of nutrients in waters below the surface mixed layer are generally not greatly influenced by the growth of

phytoplankton. They therefore provide a good indicator of the resources for phytoplankton growth that can be mixed into the water column during winter, or during summer and fall through upwelling. Thus, only the mid-layer nutrient inventory distribution is presented for the GSL (Figs. 15, 16). All nutrient concentrations, but especially silicate concentrations, showed widespread negative anomalies in summer, with N:P ratios being mostly below normal in eGSL (Fig. 15). During fall, nitrate and silicate concentrations and N:P ratios were generally below normal in eGSL while silicate concentrations were well above normal in the Estuary (Fig. 16).

The chl *a* anomaly pattern was highly variable between seasons and subregions in 2017. Overall, average chl *a* concentrations were below normal in wGSL, near-normal in eGSL, and above normal in sGSL. In the latter, the positive anomaly is the highest recorded since 2002 (Fig. 13). The distribution of chl *a* concentrations in summer shows how widespread this positive anomaly was within sGSL and around the Gaspé Peninsula (Fig. 17). However, this strong positive anomaly was not observed at Shediac Valley station, where a positive anomaly for surface layer nitrate was recorded (Fig. 7e). Inconsistencies could be related to the timing of the AZMP surveys relative to the spring bloom phenology, or to the infrequent sampling at Shediac Valley station, so we must be cautious with our interpretation. During fall, the mouth of Chaleur Bay was associated with a strong positive chl *a* anomaly while chl *a* concentrations were mostly near normal elsewhere (Fig. 17).

Remote sensing of ocean colour

Satellite imagery suggests that the start of the spring bloom was generally on time in all statistical subregions, but the maximum chl *a* concentration reached during the bloom (amplitude) was below normal in most areas (Fig. 18). In the northwest GSL, even though the bloom started on time, the peak of the bloom was delayed and strong positive anomalies of surface chl *a* were seen in late May – early June (Figs. 18, 19). In the Magdalen Shallows, the spring bloom typically seen in April was very weak, with negative surface chl *a* anomalies seen over the whole sGSL. Phytoplankton biomass finally accumulated in the surface waters in June and was above or near normal thereafter (Figs. 18, 19). Statistical estimations of spring bloom parameters show that amplitude and magnitude were generally below normal throughout the GSL (Fig. 20). The longer duration of the bloom in the northwest GSL, owing to an on-time start and a delayed bloom peak, was responsible for the above-normal magnitude of the bloom there. Interestingly, these bloom parameter estimates, which are based on a shifted Gaussian function (Zhai et al. 2011), suggest earlier timing of the bloom in all subregions (Fig. 20), whereas field observations suggest a near-normal timing (Fig. 18). The spring bloom was likely too small in the Magdalen Shallows during 2017 to calculate spring bloom parameters (Figs. 18, 20).

Surface phytoplankton biomass was generally near normal during fall over the GSL, as was the annual biomass average (Figs. 20, 21). Interestingly, several negative anomalies have been observed over various regions and seasons since 2012 in comparison with previous years. The positive anomalies observed in summer 2017 in the Magdalen Shallows and Cabot Strait and in NWGSL in fall are actually the first positive anomalies recorded since 2012. Overall, the composite images (Figs. 19, 21) agree well with field data (Fig. 17), except in the eastern sGSL where field data show positive anomalies in early June and composite images show near-normal biomass values. The minor discrepancies between methods are likely attributable to the difference in chl *a* vertical integration. As noted above, satellite imagery estimates only the near-surface layer, whereas the shipboard data integrate the top 100 m of the water column.

ZOOPLANKTON

High-frequency monitoring sites

In 2017, the zooplankton biomass at both Rimouski and Shediac Valley stations were near or below normal all year long, with one exception in late fall at Rimouski station (Fig. 22). The pattern at Rimouski station was similar to the climatology: there was an increase in biomass over the season, although biomass kept increasing during fall when it usually remains stable or diminishes slightly (Fig. 22a). Sampling frequency at Shediac Valley station was much lower compared to Rimouski station (7 vs. 34 visits) and might not reveal a comprehensive seasonal pattern. Despite low biomass, total copepod abundance was near normal at Rimouski station (Fig. 23a), with the seasonal variability in the copepod assemblage notably different from the long-term climatology (Fig. 23). While *Calanus glacialis* and *Pseudocalanus* spp. appear in the climatology, they were not in the top 95% in 2017. *Calanus* spp, which dominated the copepod assemblage from early spring to early fall during the reference period, were replaced by an increased relative abundance of smaller species such as *Microcalanus* spp. and *Triconia borealis* in 2017 (Fig. 23). At Shediac Valley, low biomass was associated with lower-than-normal copepod abundance (Fig. 24a). While the copepod assemblage at Shediac Valley in 2017 was relatively similar to the reference period (Fig. 24b, c), there were several newcomers among the dominant taxa in 2017, including small copepods as well as *Triconia borealis* that contributed significantly to total copepod abundance. *Calanus glacialis* was not part of the dominant copepod species in 2017, and the relative abundance of *C. hyperboreus* diminished considerably (Fig. 24b, c). This large decrease in the relative abundance of *Calanus* spp. compared to the long-term average at both sites is driven by both an increase in abundance of smaller taxa (*Triconia borealis* at both sites; *Microcalanus* spp. at Rimouski station) and a decrease in *Calanus* spp. abundance at both sites (Figs. 23, 24).

Calanus finmarchicus abundance in 2017 was below the long-term seasonal average at Rimouski station (Fig. 25a). The contribution of early copepodite stages (CI–CIII) was below normal during early summer, and they peaked in early July (Fig. 25c) whereas their maximum contribution is typically seen in mid-June (Fig. 25b).The late summer increase in the proportion of adults and CI–CIII suggests the possible occurrence of a second generation (Fig. 27c). Similarly, at Shediac Valley station, *C. finmarchicus* abundance was below normal during most of 2017 (Fig. 25d) and the contribution of early copepodite stages was smaller than normal during summer (Fig. 25e, f).

The abundance of the large-bodied *C. hyperboreus* was above the long-term average at the onset of the productive season and below thereafter at Rimouski station (Fig. 26a). The relative contribution of adult (CVI stage) to total abundance in 2017 was less than during the reference period, and copepodite stage CV was the dominant stage most of the year (Fig. 26b, c). Overall, the stable stage structure from July onward at Rimouski station indicates a population in diapause, mainly at stage CV. *Calanus hyperboreus* abundance was also below normal in 2017 at Shediac Valley station (Fig. 26d), where the contribution of early stages in May was almost half the average for the reference period (Fig. 26e, f). No *C. hyperboreus* were detected in fall, which limits our capacity to describe the seasonal pattern of stage composition at this site (Fig. 26f).

The abundance of *Pseudocalanus* spp. at Rimouski station was near normal during spring 2017 and below normal thereafter despite a strong peak of early copepodite stages in mid-May (Fig. 27a, c). The timing of this early stage peak was similar to the climatology (Fig. 27b, c). No adults were found in samples collected during fall (Fig. 27c); adults typically account for about 15% of total abundance at this time of the year at Rimouski station (Fig. 27b). At Shediac Valley,

Pseudocalanus spp. abundance was also below the long-term average most of the year (Fig. 27d). No stage analysis was carried out for these species at Shediac Valley station.

Gulf subregions

As observed at the high-frequency sampling stations, the average total zooplankton biomasses during spring and fall 2017 were among the lowest seen over the 2000–2017 period in wGSL and sGSL (Fig. 28). In eGSL, spring biomass was the highest measured since 2013 while fall biomass was among the lowest recorded over the time series (Fig. 28). In wGSL, *C. finmarchicus* abundance reached a record low during spring while fall abundance was the second lowest observed over the time series. Its abundance was also very low in sGSL during both seasons while it reached a record high in eGSL in spring (Fig. 29). This record high was associated with a peak in CI–CIII abundance (data not shown), suggesting that sampling occurred when total abundance was likely the highest of the season. Total abundance of *C. hyperboreus* was relatively similar to what has usually been observed since 2000 for both seasons in wGSL and eGSL and for fall in sGSL. However, its abundance in spring 2017 was much lower than normal for the third consecutive year in sGSL (Fig. 30). *Pseudocalanus* spp. abundance has been on the rise recently in all GSL subregions (Fig. 31). However, its abundance generally dropped in 2017 in all subregions, with the exception of eGSL and sGSL in fall. The patterns of interannual variability for these three key copepod taxa generally agree well with those observed at the high-frequency monitoring stations (cf. Rimouski station and wGSL, Shediac Valley station and sGSL), considering their generally low abundance at both stations (Figs. 25–27a, d). Moreover, the high abundance of *Pseudocalanus* spp. in sGSL during the fall survey is consistent with its higher-than-normal abundance in November at Shediac Valley station (Fig. 27d).

Copepod phenology

To indicate changes in the developmental timing of zooplankton in the GSL, we present the detailed seasonal pattern (from 1994 to 2017) at Rimouski station of the relative copepodite stage proportions of *C. finmarchicus,* a key copepod species (Fig. 32). Overall, there is an obvious ongoing trend towards earlier population development. However, developmental timing in 2017 was late in comparison with recent years. Indeed, the pulse of adult stage (CVI) in late June was among the latest observed since 1994, suggesting a late emergence from diapause. Consequently, the timing of the early copepodite stages (CI–CIII) peak in 2017 occurred at the same time as that of the second generation of early copepodite stages in recent years. The relatively large contribution of the adult stage to the population in August suggests the occurrence of a second generation even though cohort development was late in 2017 (Fig. 32).

Scorecards

The time series of annual anomalies for zooplankton biomass highlights recent drastic changes in the community, with mostly negative anomalies across the GSL since 2010 (Fig. 33). In 2017, record lows of zooplankton biomass were measured in wGSL and at Shediac Valley station while the second lowest of the time series was seen in sGSL. A synthesis of standard AZMP zooplankton indices (abundance of *C. finmarchicus*, *Pseudocalanus* spp., total copepods, non-copepods) was performed using annual standardized abundance anomalies and is presented as a scorecard (Fig. 34). The negative anomalies for *C. finmarchicus* in 2017 in almost all GSL subregions were a continuation of a pattern initiated in 2009. In contrast, the pattern of *Pseudocalanus* spp. positive anomalies that began approximately at the same period was interrupted in 2017 by negative anomalies everywhere but in eGSL. Similarly, negative anomalies for total copepods were observed in most subregions in 2017, a first since 2013.

Finally, non-copepod abundance was above normal in eGSL and sGSL, continuing a trend observed since 2011. In wGSL, however, their abundance was below normal for the first time since 2013 (Fig. 34).

The annual standardized abundance anomalies for six additional zooplankton indices (*C. hyperboreus* and five zooplankton groups: small calanoids, large calanoids, cyclopoids, warm-water species, and cold/arctic species) are presented in Figure 35. *Calanus hyperboreus* was below normal in sGSL and eGSL in 2017; such negative anomalies have been observed frequently in these two regions since 2010. In relation with the trends observed for *C. finmarchicus* and *Pseudocalanus* spp., there has been a decline in large calanoid abundance and a rise in small calanoid abundance since 2009 (Fig. 35). Positive anomalies for small calanoids were again observed in 2017 at Rimouski station and in eGSL, but a negative anomaly was observed at Shediac Valley station. The exact same anomaly pattern was observed for cyclopoids (including *Triconia/Oncaea*) as for small calanoids in 2017. Negative anomalies for large calanoids were observed across the GSL, except in eGSL. Widespread positive anomalies for warm-water-associated copepods were observed again in 2017; this trend has predominated since 2009. The strongest anomaly was found in wGSL, which is where the strongest anomalies have been observed in recent years (Fig. 35). Cold-water copepods were generally below normal in 2017, except in eGSL. It must be noted that indices of warm-water and cold/arctic species are based on generally rare taxa, implying that relatively minor changes in abundance could result in large variations in their anomalies. Interestingly, all zooplankton indices except *C. hyperboreus* abundance showed positive anomalies in eGSL (Figs. 34, 35). Again this year, these annual anomalies were relatively coherent among the high-frequency sampling sites (Rimouski and Shediac Valley stations) and their associated GSL subregions (Figs. 34, 35).

DISCUSSION

ENVIRONMENTAL CONDITIONS

The timing of the onset and the extent of water column stratification play a role in defining spring bloom phenology, phytoplankton production, species succession, and trophic interactions over the full growth season (Levasseur et al. 1984). In 2017, the annual average freshwater runoff of the St. Lawrence River was at its highest level since 1974 (Galbraith et al. 2018), and it was clearly responsible for the very strong stratification observed at Rimouski station during spring and at Shediac Valley station during summer. In addition to the effect of water column stratification on phytoplankton dynamics, thermal properties of the surface, intermediate (Cold Intermediate Layer [CIL], 30–125 m), and deep-water masses play a role in defining zooplankton dynamics (Plourde et al. 2002). Galbraith et al. (2018) reported on the physical conditions that prevailed in the GSL during 2017, and this document reports on the chemical and biological conditions in the GSL in the context of these conditions.

Changes in dissolved oxygen of the deep waters entering the GSL at the continental shelf are related to the varying proportions of Labrador Current water (cold/fresh, high dissolved oxygen levels) and slope water (warm/salty, low dissolved oxygen levels), which together are the source of GSL deep water (McLellan 1957, Lauzier and Trites 1958, Gilbert et al. 2005). These waters travel from the mouth of the Laurentian Channel to the Estuary in roughly three to four years (Gilbert 2004), decreasing in dissolved oxygen as a result of *in situ* respiration and oxidation of organic material as they progress to the channel heads. Based on interdecadal variability, the inflow of warmer waters to the Estuary is expected to exacerbate the hypoxic conditions since these waters are typically poorer in dissolved oxygen (McLellan 1957, Lauzier and Trites 1958, Gilbert et al. 2005). Several factors are at play in the determination of dissolved oxygen in

waters entering the Gulf of St. Lawrence, including bacterial activity and temperature. The latter is particularly significant. In the St. Lawrence Estuary, it has previously been shown that temperature explains 74% of oxygen variability over the time series (Galbraith et al. 2017).A change in dissolved oxygen of 147.4 µM can be accounted for by a 10.09°C temperature difference in source water masses (Gilbert et al. 2005), implying that a decrease of 1.46 µM might be expected for each 0.1°C temperature increase observed at Cabot Strait due to the variability of the mixing ratio of source waters. However, during the last three years, the average deep dissolved oxygen concentration has been about 23 µM lower than during the reference period in Cabot Strait region for an associated increase in temperature of ca. 0.5°C. Thus, warming of bottom water is not the only factor accountable for the decrease in oxygen concentrations in the GSL. Other factors that can cause oxygen variability include interannual changes in the vertical flux of organic matter to the bottom waters of the Lower St. Lawrence Estuary.

Winter mixing is a critical process for bringing nutrient-rich deep water to the surface. In the GSL, this winter convection is partly caused by buoyancy loss attributable to cooling and reduced freshwater runoff, brine rejection associated with sea-ice formation, and wind-driven mixing prior to ice formation (Galbraith 2006). Warm surface waters throughout the winter and minimal sea-ice formation imply low winter convection and may reduce the amount of nutrients available for spring production. Negative nitrate anomalies in the surface layer have been regularly encountered in the GSL since 2010, a period over which several temperature and ice cover indices have shown clear warming of the GSL (Galbraith et al. 2018). The CIL is the winter surface mixed layer that has been insulated from the atmosphere by near-surface stratification and whose nutrient inventory will supply primary producers during the growth season through upwellings. Thus, weak winter convection during 2017 also explains the widespread negative nutrient anomaly in the mid-layer during June. Strong stratification during the first part of the growth season might have limited upwelling in regions under the influence of freshwater (wGSL and sGSL) and allowed a return to near-normal conditions in fall in these regions.

Positive anomalies in deep-water (300 m) nutrients have been observed since 2012 in eGSL in association with high temperature and salinity intrusions into the GSL from Cabot Strait (Galbraith et al. 2018). These higher-than-average deep inventories are probably also associated with a combination of a thermocline that is shallower and a water mass composition that has a greater contribution of slope water than Labrador Shelf water (Galbraith et al. 2018). In contrast, deep-water negative nutrient anomalies were observed at Rimouski station for a second consecutive year, and possibly elsewhere in the Estuary. These could be the result of changes in the activity of bacteria involved in the nitrogen cycle, such as decreased nitrification associated with low oxygen concentrations. Routine measurement of NH_4 concentration has recently been added to AZMP sampling in the GSL and will eventually be helpful to verify these hypotheses. Moreover, modelization of processes involved in the nitrogen cycle in the GSL is ongoing (Diane Lavoie, IML) and will allow understanding of key processes involved in nitrate distribution.

The N:P ratio is another index that requires further attention since variability in the stoichiometries of nutrient supply is a key determinant of oceanic nutrient limitation. Thus, changes in the CIL N:P ratio over time may be a better predictor of changes in the phytoplankton community and productivity than nitrate concentrations themselves. Thus, if the negative anomalies in the N:P ratio in eGSL in 2017 were to persist through time, they might entail a change in the productivity of this region.

PHYTOPLANKTON

Except at Rimouski station, where sampling regularly covers the spring bloom period, phytoplankton productivity during the spring bloom must be inferred either from indirect indices collected at sea, such as the difference in nutrient inventory of the surface mixed layer between the winter and the spring cruises, or from satellite observations. Interestingly, nutrient drawdown associated with spring productivity was below normal in 2017 in regions that are under the direct influence of freshwater discharge from the St. Lawrence River (Ohashi and Sheng 2013) but near normal elsewhere. Based on this index, a possible massive input of nutrients associated with the strong 2017 freshet could mistakenly suggest low spring productivity in wGSL and the western portion of sGSL. However, satellite observations during the spring bloom tend to confirm the occurrence of a generally low amplitude and low magnitude bloom across the GSL. The timing and intensity of the spring bloom in the St. Lawrence Estuary is known to be largely influenced by both runoff intensity and freshwater-associated turbidity (Levasseur et al. 1984, Therriault and Levasseur 1985, Zakardjian et al. 2000, Le Fouest et al. 2010, Mei et al. 2010). In the regions most influenced by the outflow of the St. Lawrence River, the strong discharge of freshwater—and presumably of particulate material in suspension that may have increased turbidity—may have prevented phytoplankton biomass accumulation by either flushing it further downstream or by limiting phytoplankton growth through reduced light availability.

However, bloom statistics estimated from the Gaussian function (Zhai et al. 2011) suggest that the magnitude of the bloom was above normal in wGSL because it lasted longer, and it also suggests an early start of the bloom across the GSL. This contrasts with the observations themselves (Fig. 18), which showed that bloom timing in 2017 was similar to the long-term average and that the bloom in wGSL was not necessarily longer but rather that the peak was delayed. The effect of low spring biomass, such as was measured in 2017 across the GSL, on the accuracy of certain bloom parameter estimations, especially the start of the bloom (which is defined as the date when chl *a* concentration reaches 20% of the amplitude of the bloom; Zhai et al. 2011), would require further investigation as to whether it might introduce biases. The annual biomass average was near normal according to satellite observations, with strong positive anomalies of chl *a* during summer in sGSL that were confirmed by field data. The low zooplankton biomass, as observed throughout the GSL in 2017, and reduced grazing pressure could have allowed growth of phytoplankton to above-normal values despite a relatively weak spring bloom in this region. Those summer anomalies in sGSL are the first positive anomalies recorded since we began using VIIRS satellite data in 2012. It is possible that the VIIRS satellite performs better in coastal waters in terms of minimizing the overestimation of chl *a* concentration in turbid waters compared with previous satellites. If so, this could partly explain why most satellite-derived biomass estimate anomalies have been negative since the use of this satellite in 2012. Improved algorithms for the retrieval of chl *a* in the Gulf of St. Lawrence from the SeaWIFS satellite have recently been published (Laliberté et al. 2018) and should eventually be applied to our statistical subregions; this could modify the time series anomaly pattern.

Diatoms are typically found in nutrient-rich, well-mixed environments because they mainly rely on nitrate to fulfill their nitrogen requirement; smaller-sized cells such as flagellates and dinoflagellates are associated with nutrient-poor, stratified environments and mostly use reduced forms of nitrogen, such as ammonium (Levasseur et al. 1984, Li and Harrison 2008). Thus, the highly stratified environment that prevailed at Rimouski station during spring and at Shediac Valley station during summer—and likely elsewhere in wGSL and sGSL over the same seasons—was probably favourable to flagellated phytoplankton communities. The AZMP program has not regularly documented the taxonomic composition of the phytoplankton community elsewhere in the GSL, and we must be cautious when generalizing these results to

other GSL subregions. Nevertheless, flagellate-dominated communities could be responsible for low phytoplankton biomass at both high-frequency monitoring stations and in wGSL during 2017. Notwithstanding overall flagellate dominance in 2017, diatoms were responsible for the strong late-summer bloom recorded at Rimouski station. A second phytoplankton bloom can occur when late summer/early fall winds are strong enough to break the stratification and upwell deep nutrient-rich waters to the sea surface. Observations of the vertical profiles of salinity (see Fig. 63 in Galbraith et al. 2018) and nitrate recorded at Rimouski station showed that the strong fall bloom was preceded by the intrusion of saltier, nutrient-rich water from greater depths into the surface layer. Thus, environmental parameters altering the onset of stratification and its strength throughout the productive season could possibly play a critical role in determining annual phytoplankton biomass, community composition, and the possibility for the occurrence of a second bloom.

ZOOPLANKTON

Among the most striking features in 2017 was the very low zooplankton biomass for a third consecutive year throughout the GSL, except in eGSL during spring. Depending on the subregion, this biomass level can be roughly estimated as a decrease of between 2 and 4 g C m^{-2} compared with the long-term average. In sGSL, this represents a drop of ca. 90% of the long-term mean total biomass. Lower biomass is likely associated with the decrease in large-sized zooplankton species abundance, particularly in sGSL. The mean weight of large-sized calanoids (e.g., *C. hyperboreus,* 4 g per adult female) is between one and two orders of magnitude larger than that of small-sized calanoids (e.g., *Pseudocalanus* spp., 0.02 g per adult female) (Conover and Huntley 1991). Thus, the diminution of large calanoid abundance will have a greater impact on zooplankton biomass than, for instance, the decrease of *Pseudocalanus* spp. abundance that was recorded in most GSL subregions in 2017.

The small spring bloom amplitude, the lower contribution of diatoms to the phytoplankton assemblage at the onset of the growth season, and the delay in the accumulation of phytoplankton biomass may all have contributed to the widespread negative anomalies of the large calanoid index. Moreover, it has been hypothesized that high spring freshwater runoff from the St. Lawrence River, which was observed in 2017, could result in a lower transport of *Calanus* species to sGSL (Runge et al. 1999, Galbraith et al. 2018), especially when considering their low abundance at Rimouski station during spring. Life cycle strategies are different among large copepod species, and the timing of reproduction relative to the freshet—considering its influence on water-mass circulation and transport—could explain dissimilarities in the distribution pattern of these species, for instance strong negative anomalies of *C. finmarchicus* versus near-normal abundance of *C. hyperboreus* in wGSL. Increased predation pressure in the northern GSL by massive successive cohorts of largely planktivorous local redfish (*Sebastes mentella*) could also have persisted in 2017 (Bourdages et al. 2017). However, quantitative assessment of the predatory impact of redfish on large copepods are lacking in the GSL to validate this hypothesis.

For the first time since 2013, *Pseudocalanus* spp. and total copepod abundances were below normal in sGSL and wGSL, as was non-copepod abundance in wGSL and the cyclopoid index at Shediac Valley. All these indices have mostly shown widespread positive anomalies since 2008, suggesting a general shift towards smaller zooplankton species with potential implications for the pelagic food web and pelago–benthic coupling. This change towards a dominance of smaller taxa was mainly attributable to *Pseudocalanus* spp. and may have been explained by the sustained below-normal abundance of *C. finmarchicus* (since 2009) throughout the GSL, which could have favoured the recruitment of *Pseudocalanus* spp. by diminishing competition for adequate food. Indeed, reverse anomaly patterns can be seen for these two copepod taxa

over the study period (1999–2016; Fig. 34) and may suggest that competition is occurring between the species. However, it seems that environmental conditions in 2017 were unfavourable for the growth of most zooplankton groups, including *Pseudocalanus* spp., in almost all GSL subregions. The only exception is in eGSL, where all zooplankton indices except *C. hyperboreus* showed positive anomalies. A stronger Gaspé Current resulting from an exceptional St. Lawrence River discharge (Ohashi and Sheng 2013) could potentially have facilitated the export of zooplankton from wGSL to eGSL. Furthermore, eGSL was likely the subregion the least affected by the input of freshwater that altered stratification and modified the assemblage and timing of food resources in other subregions, suggesting that growth conditions were possibly better in this subregion compared with others. Interestingly, *Pseudocalanus* spp. showed positive anomalies everywhere along the Newfoundland and Labrador sections in 2017, and the two southernmost sections were also associated with positive *C. finmarchicus* anomalies (DFO 2018). Thus the favourable environmental conditions that prevailed along the Newfoundland and Labrador Shelf might also have enhanced the survival and growth of these copepods in eGSL.

The year-round warm temperature of the whole water column in 2017 may also have driven some changes in community composition. Warm-water copepod species showed strong positive anomalies almost everywhere in 2017, particularly in wGSL. In most regions, these anomalies were largely driven by *Metridia lucens* (data not shown). *Centropages* spp. was also a major contributor to these positive anomalies in sGSL and eGSL (data not shown). *M. lucens* is a strong vertical migrator that is mostly associated with temperate conditions. Thus, it might have benefited from a warmer and saltier deep layer as well as from warmer conditions at the surface that have become typical in the GSL in recent years. Despite generally warm conditions, eGSL has shown positive anomalies for cold/arctic copepod species most of the time since 2007, including in 2017. This is mostly because of the relatively high abundance of *M. longa* (data not shown). Their mesopelagic early copepodite stages are known to exploit sinking phytoplankton aggregates and associated microfauna (Grønvik and Hopkins 1984, Plourde et al. 2002). The ice algae that may bloom underneath the ice entering the GSL through the Strait of Belle Isle during spring could represent an interesting food source for this cold-adapted species (Tremblay et al. 1989) as well as for *C. glacialis* females, who are known to utilize the high-quality ice algal bloom to fuel early maturation and reproduction (Søreide et al. 2010). In 2017, ice advection through the Strait of Belle Isle led to the highest ice volume during June since 1969 (Galbraith et al. 2018). Temperatures in the surface layer and CIL were also below normal most of the year in some small regions within eGSL, such as Mecatina Trough (see Fig. 55 in Galbraith et al. 2018), which may also have been beneficial to the growth of cold/arctic species in eGSL. However, these causal relationships between environmental conditions and zooplankton community composition have not been addressed yet in the context of the AZMP program and they remained hypothetical.

In addition to their possible effect on the zooplankton assemblage, local environmental conditions might also have resulted in a late timing of *C. finmarchicus* development in 2017 compared to previous years at Rimouski station, with potential consequences on upper trophic levels. At Rimouski station, the late onset of the spring bloom as a result of the strong stratification probably caused late reproduction and reduced offspring survival and development. Growth and development of *Pseudocalanus* spp. also depend on phytoplankton bloom phenology, but their copepodite assemblage at Rimouski station revealed that its developmental timing in 2017 was highly similar to the reference period. However, the near absence of early stages during fall also suggests reduced offspring survival and slower development for this taxon. The decreased proportion of adults (copepodite stage CVI) in *C. hyperboreus* populations at Rimouski station in 2017, which has also regularly been seen during fall since 2009 in wGSL and eGSL (data not shown), suggests that changes are also occurring in the life

cycle of *C. hyperboreus*. Indeed, it could indicate a diminution in the proportion of multiparous females that typically have a multiannual life cycle. Overall, zooplankton communities in the GSL seem to be shaped by a combination of changing water-mass properties and of bottom-up and top-down controls, although the relative importance of these factors is not yet well understood.

SUMMARY

This document reports on the chemical and biological (plankton) conditions in the GSL in 2017 in the context of a strong warming event initiated in 2010. Data from 2017 are compared to time-series observations.

- Strong stratification of the upper water column during spring and summer at Rimouski and Shediac Valley stations, respectively, was caused by the unusually large spring freshet.
- Concentrations of dissolved oxygen strongly decreased in the Gulf in 2017, reaching the lowest observed values since 2000 in all regions but the northwest GSL.
- Surface nitrate inventories (0–50 m) were generally near the long-term average most of the year in all GSL subregions despite low winter convection. Strong positive deep-water (> 200 m) nutrient anomalies have been observed since 2012 in eGSL and are associated with intrusions of high temperature/high salinity water into the GSL through Cabot Strait.
- According to satellite imagery, the amplitude and magnitude of the spring bloom were generally below normal throughout the GSL. Small nutrient drawdown between winter and summer sampling in wGSL and around the Gaspé Peninsula corroborates these observations.
- At Rimouski station, the delay of the spring bloom was caused by the accumulation of freshwater in the surface layer and strong stratification. Except for the short spring and late summer blooms, phytoplankton biomass stayed below normal all year long. At Shediac Valley station, the annual biomass was near normal. The contribution of diatoms to the phytoplankton assemblage was lower than during the reference period at these two sites.
- Zooplankton biomass was below normal in 2017 throughout the GSL during spring and fall because of decreases of the large-bodied C. finmarchicus in wGSL and sGSL and of C. hyperboreus in eGSL and sGSL. Pseudocalanus spp. also exhibited negative anomalies in most regions, which is a first since 2007.
- Adverse growth conditions in wGSL and sGSL, including reduced food resources and increased predation pressure, are among the hypotheses that could explain low zooplankton biomass and abundance in these regions. On the contrary, almost all zooplankton indices showed positive anomalies in eGSL, which could hypothetically be explained by the advection of zooplankton into eGSL from source regions via an unusually strong Gaspé Current and/or by the advection of sea-ice that may have been used as a food source (ice algae) by cold-adapted species.
- Positive anomalies in the warm-water copepod index were measured throughout the GSL in 2017 and were particularly strong in wGSL, associated with the increased abundance of M. lucens.
- Local conditions at Rimouski station have delayed the timing of *C. finmarchicus* development compared to previous years, with potential consequences on upper trophic levels. In 2017, this keystone species showed the most delayed development since 2005.

ACKNOWLEDGEMENTS

We thank Jean-Yves Couture, Marie-France Beaulieu, Caroline Lebel, Isabelle St-Pierre, and Caroline Lafleur for preparation and standardization of the phytoplankton and zooplankton data. The data used in this report would not be available without the work of François Villeneuve and his AZMP team (Rémi Desmarais, Marie-Lyne Dubé, Yves Gagnon, Line McLaughlin, Roger Pigeon, Michel Rousseau, Félix St-Pierre, Liliane St-Amand, Sonia Michaud, David Leblanc, and Caroline Lafleur) in organizing and carrying out AZMP surveys and analyzing samples. We thank Jeff Spry and Kevin Pauley for providing data from the Shediac Valley station and BIO's remote sensing unit for the composite satellite images. We are grateful to Pierre Pepin and Emmanuel Devred for their critical reviews.

REFERENCES

Arun Kumar, S.V.V., Babu, K.N., and Shukla, A.K. 2015. Comparative analysis of chlorophyll-a distribution from SeaWiFS, MODIS-Aqua, MODIS-Terra and MERIS in the Arabian Sea. Mar. Geod. 38: 40–57.

Barnes, B., and Hu, C. 2016. Dependence of satellite ocean color data products on viewing angles: A comparison between SeaWiFS, MODIS, and VIIRS. Remote Sens. Environ. 175: 120–129.

Bourdages, H., Brassard, C., Desgagnés, M., Galbraith, P., Gauthier, J., Légaré, B., Nozères, C., and Parent, E. 2017. Preliminary results from the groundfish and shrimp multidisciplinary survey in August 2016 in the Estuary and northern Gulf of St. Lawrence. DFO Can. Sci. Advis. Sec. Res. Doc. 2017/002. v + 87 p.

Brickman, D., and Petrie, B. 2003. Nitrate, silicate and phosphate atlas for the Gulf of St. Lawrence. Can. Tech. Rep. Hydrogr. Ocean Sci. 231: xi + 152 pp.

Conover, R. J., and Huntley, M. 1991. Copepods in ice-covered seas - Distribution, adaptations to seasonally limited food, metabolism, growth patterns and life cycle strategies in polar seas. J. Mar. Syst. 2: 1–41.

DFO. 2018. Oceanographic conditions in the Atlantic zone in 2017. DFO Can. Sci. Advis. Sec. Sci. Advis. Rep. 2018/039.

Galbraith, P. S. 2006. Winter water masses in the Gulf of St. Lawrence. J. Geophys. Res. 111, C06022, doi: 10.1029/2005JC003159.

Galbraith, P. S., Desmarais, R., Pigeon, R., and Cantin, S. 2006. Ten years of monitoring winter water masses in the Gulf of St. Lawrence by helicopter. AZMP Bulletin PMZA 5: 32–35.

Galbraith, P.S., Chassé, J., Caverhill, C., Nicot, P., Gilbert, D., Pettigrew, B., Lefaivre, D., Brickman, D., Devine, L., and Lafleur, C. 2017. Physical oceanographic conditions in the Gulf of St. Lawrence in 2016. DFO Can. Sci. Advis. Sec. Res. Doc. 2017/044. v + 91 p.

Galbraith, P.S., Caverhill, C., Chassé, J., Nicot, P., Gilbert, D., Lefaivre, D., and Lafleur, C. 2018. Physical oceanographic conditions in the Gulf of St. Lawrence in 2017. DFO Can. Sci. Advis. Sec. Res. Doc. 2018/050. v + 79 p.

Gilbert, D. 2004. Propagation of temperature signals from the northwest Atlantic continental shelf edge into the Laurentian Channel. ICES CM, 2004/N: 7, 12 pp.

Gilbert, D., Sundby, B., Gobeil, C., Mucci, A., and Tremblay, G.-H. 2005. A seventy-two-year record of diminishing deep-water oxygen in the St. Lawrence estuary: The Northwest Atlantic connection. Limnol. Oceanogr., 50(5): 1654–1666.

Gregg, W. W., and Rousseaux, C. S. 2014. Decadal trends in global pelagic ocean chlorophyll: A new assessment integrating multiple satellites, in situ data, and models. J. Geophys. Res. Oceans, 119: 5921–5933, doi 10.1002/2014JC010158.

Grønvik, S., and Hopkins, C. C. E. 1984. Ecological investigations of the zooplankton community of Balsfjorden, northern Norway: Generation cycle, seasonal vertical distribution, and seasonal variations in body weight and carbon and nitrogen content of the copepod *Metridia longa* (Lubbock). J. Exp. Mar. Biol. Ecol. 80: 93–107.

Johnson, C., Casault, B., Head, E., and Spry, J. 2016. Optical, chemical, and biological oceanographic conditions on the Scotian Shelf and in the Eastern Gulf of Maine in 2014. DFO Can. Sci. Advis. Sec. Res. Doc. 2016/003. v + 51 p.

Laliberté, J., Larouche, P., Devred, E., and Craig, S. 2018. Chlorophyll-a concentration retrieval in the optically complex waters of the St. Lawrence Estuary and Gulf using principal component analysis. Remote Sens. 10, 265, doi: 10.3390/rs10020265.

Lauzier, L.M., and Trites, R.W. 1958. The deep waters of the Laurentian Channel. J. Fish. Res. Board Can. 15: 1247–1257.

Le Fouest, V., Zakardjian, B., and Saucier, F. J. 2010. Plankton ecosystem response to freshwater-associated bulk turbidity in the subarctic Gulf of St. Lawrence (Canada): A modelling study. J. Mar. Syst. 81(1-2): 75–85.

Levasseur, M., Therriault, J.-C., and Legendre, L. 1984. Hierarchical control of phytoplankton succession by physical factors. Mar. Ecol. Prog. Ser. 19: 211–222.

Li, W. K. W., and Harrison, W. G. 2008. Propagation of an atmospheric climate signal to phytoplankton in a small marine basin. Limnol. Oceanogr. 53(5): 1734–1745.

McLellan, H.J. 1957. On the distinctness and origin of the slope water off the Scotian Shelf and its easterly flow south of the Grand Banks. J. Fish. Res. Board Can. 14: 213–239.

Mei, Z.-P., Saucier, F., Le Fouest, V., Zakardjian, B., Sennville, S., Xie, H., and Starr, M. 2010. Modeling the timing of spring phytoplankton bloom and biological production of the Gulf of St. Lawrence (Canada): Effects of colored dissolved organic matter and temperature. Cont. Shelf Res. 30: 2027–2042.

Mitchell, M. R., Harrison, G., Pauley, K., Gagné, A., Maillet, G., and Strain, P. 2002. Atlantic Zonal Monitoring Program sampling protocol. Can. Tech. Rep. Hydrogr. Ocean Sci. 223: iv + 23 pp.

Ohashi, K., and Sheng, J. 2013. Influence of St. Lawrence River discharge on the circulation and hydrography in Canadian Atlantic waters. Cont. Shelf Res. 58: 32-49.

Pepin, P., Maillet, G., Fraser, S., Shears, T., and Redmond, G. 2013. Optical, chemical, and biological oceanographic conditions on the Newfoundland and Labrador Shelf during 2011-12. DFO Can. Sci. Advis. Sec. Res. Doc. 2013/051. v + 38 p.

Plourde, S., Dodson, J. J., Runge, J. A., and Therriault, J.-C. 2002. Spatial and temporal variations in copepod community structure in the lower St. Lawrence Estuary, Canada. Mar. Ecol. Prog. Ser. 230: 221–224.

Plourde, S., Maps, F., and Joly, P. 2009. Mortality and survival in early stages control recruitment in *Calanus finmarchicus*. J. Plankton Res. 31(4): 371–388.

Runge, J. A., Castonguay, M., de Lafontaine, Y., Ringuette, M., and Beaulieu, J. L. 1999. Covariation of climate, zooplankton biomass and mackerel recruitment in the southern Gulf of St. Lawrence. Fish. Oceanogr. 8(2): 139–149.

Søreide, J.E., Leu, E., Berge, J., Graeve, M., and Falk-Petersen, S. 2010. Timing of blooms, algal food quality and *Calanus glacialis* reproduction and growth in a changing Arctic. Glob. Change Biol. doi: 10.1111/j.1365-2486.2010.02175.x.

Therriault, J.-C., and Levasseur, M. 1985. Control of phytoplankton production in the Lower St. Lawrence Estuary: light and freshwater runoff. Nat. Can. 112: 77–96.

Therriault, J.-C., Petrie, B., Pépin, P., Gagnon, J., Gregory, D., Helbig, J., Herman, A., Lefaivre, D., Mitchell, M., Pelchat, B., Runge, J., and Sameoto, D. 1998. Proposal for a Northwest Atlantic zonal monitoring program. Can. Tech. Rep. Hydrogr. Ocean Sci. 194: vii + 57 pp.

Tremblay, C., Runge, J. A., and Legendre, L. 1989. Grazing and sedimentation of ice algae during and immediately after a bloom at the ice-water interface. Mar. Ecol. Prog. Ser. 56: 291–300.

Wang, M., Liu, X., Tan, L., Jiang, L., Son, S. H., Shi, W., Rausch, K., and Voss, K. 2013. Impacts of VIIRS SDR performance on ocean color products. J. Geophys. Res. Atmos. 118: 10,347–10,360, doi:10.1002/jgrd.50793.

Zakardjian, B. A., Gratton, Y., and Vézina, A. F. 2000. Late spring phytoplankton bloom in the Lower St. Lawrence Estuary: the flushing hypothesis revisited. Mar. Ecol. Prog. Ser. 192: 31–48.

Zhai, L., Platt, T., Tang, C., Sathyendranath, S., and Hernández Walls, R. 2011. Phytoplankton phenology on the Scotian Shelf. ICES J. Mar. Sci. 68: 781–791, doi:10.1093/icesjms/fsq175.

Zibordi, G., Mélin, F., and Berthon, J.-F. 2006. Comparison of SeaWiFS, MODIS and MERIS radiometric products at a coastal site. Geophys. Res. Letters 33: L06617, doi:10.1029/2006GL0257.

TABLES

Table 1. List of AZMP surveys with locations, dates, and sampling activities for 2017. wGSL, eGSL, and sGSL denote the western, eastern, and southern subregions of the Gulf of St. Lawrence. See Figure 1 for station locations.

	Name	Location	Dates (2017)	Vessel	CTD/bottle	Net
Fixed	Rimouski	48º40.0'N 068º35.0'W	7 Feb – 4 Dec	Beluga II (+ others)	35	34
	Shediac Valley	47º46.8'N 064º01.8'W	11 Mar – 13 Nov	Multiple	7	7
Winter Survey	-	Estuary and Gulf	1–12 March	Earl Grey	42	20
Summer Survey	TESL	wGSL	28 May – 19 Jun	Teleost	7	7
	TSI	wGSL	28 May – 19 Jun	Teleost	6	6
	TASO	wGSL	28 May – 19 Jun	Teleost	5	5
	TIDM	sGSL	28 May – 19 Jun	Teleost	10	10
	TDC	eGSL	28 May – 19 Jun	Teleost	6	6
	TCEN	eGSL	28 May – 19 Jun	Teleost	5	4
	TBB	eGSL	28 May – 19 Jun	Teleost	7	7
Total					**46**	**45**
Fall Survey	TESL	wGSL	7–30 Nov	Coriolis II	7	7
	TSI	wGSL	7–30 Nov	Coriolis II	6	6
	TASO	wGSL	7–30 Nov	Coriolis II	5	5
	TIDM	sGSL	7–30 Nov	Coriolis II	10	10
	TDC	eGSL	7–30 Nov	Coriolis II	4	4
	TCEN	eGSL	7–30 Nov	Coriolis II	5	5
	TBB	eGSL	7–30 Nov	Coriolis II	7	7
Total					**44**	**44**

FIGURES

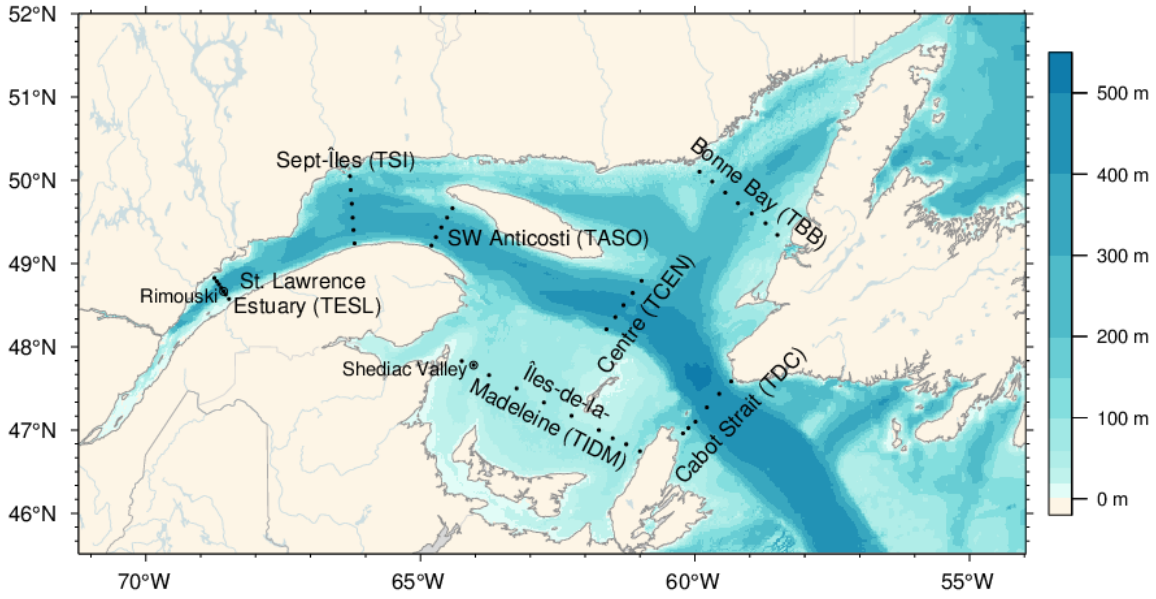

Figure 1. Bathymetric map of the Estuary and Gulf of St. Lawrence showing sampling stations on the different sections (dots) and at Rimouski and Shediac Valley stations (circles). Sections were grouped to form subregions within the western GSL: TESL, TSI, TASO; southern GSL: TIDM; and eastern GSL: TBB, TCEN, TDC.

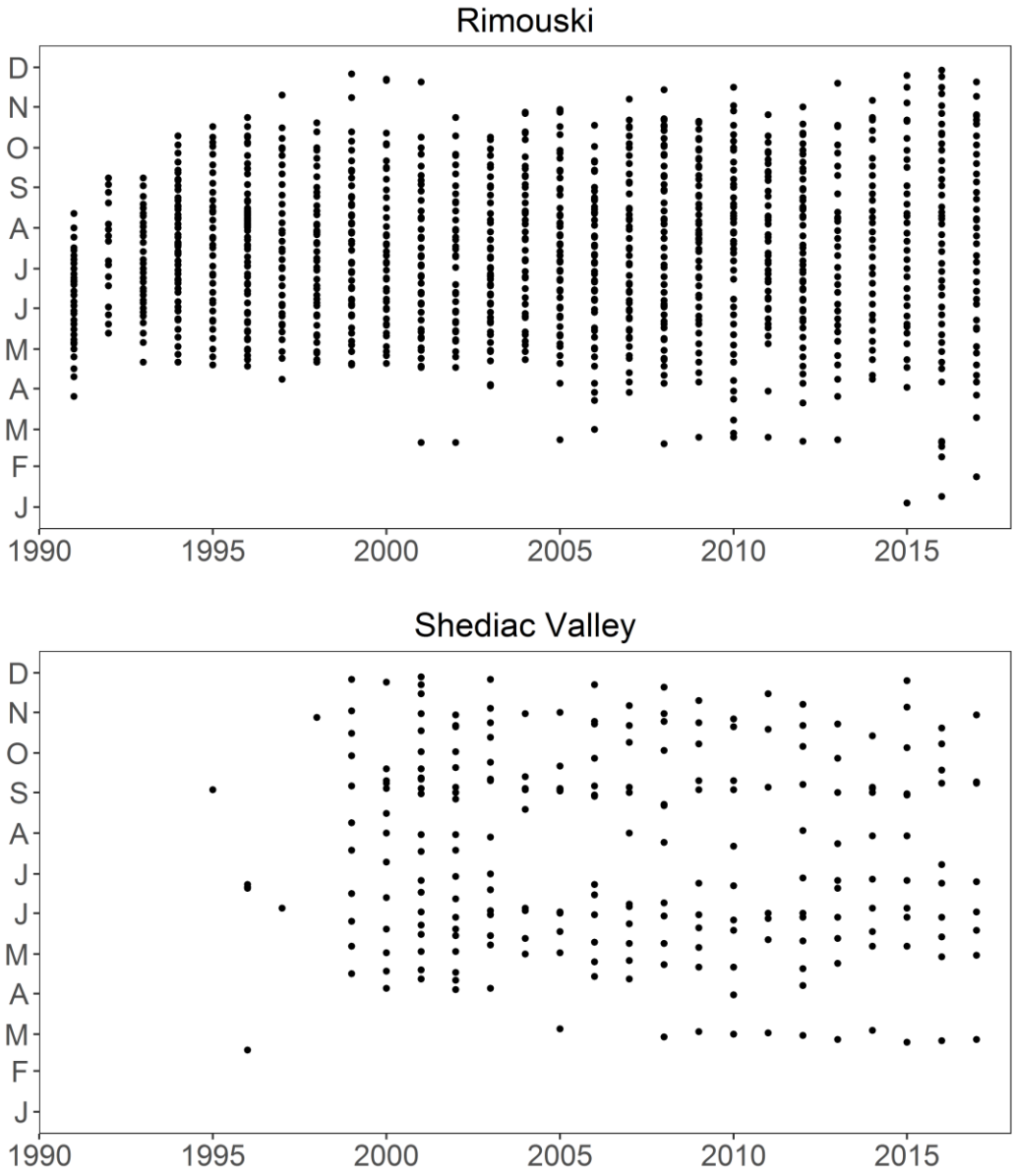

Figure 2. Sampling frequencies at Rimouski and Shediac Valley stations through 2017. Sampling included CTD/bottle as well as plankton net tows most of the time (weather permitting).

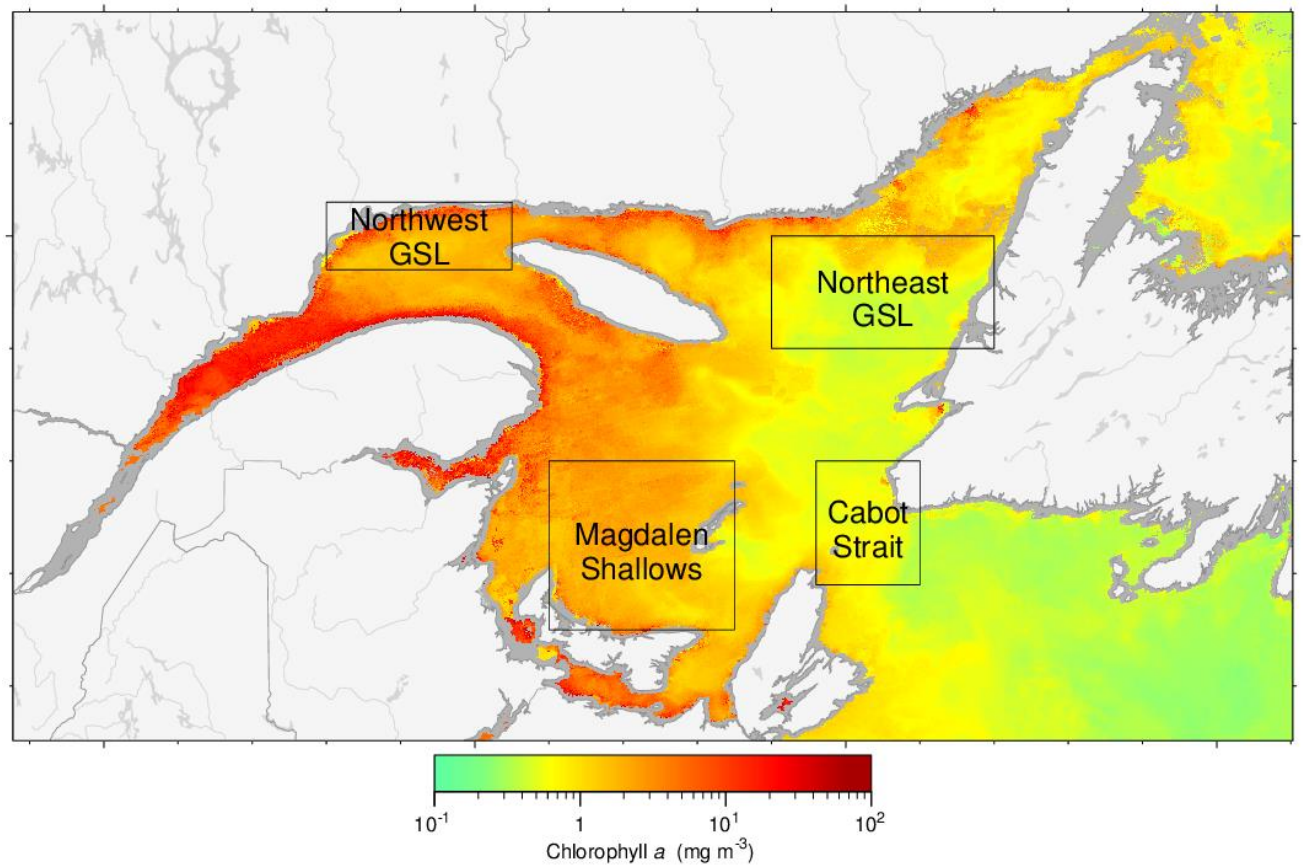

Figure 3. Statistical subregions in the GSL identified for the spatial/temporal analysis of satellite ocean colour data. The figure is a VIIRS composite image showing chlorophyll a from 16–30 June 2017. Gray areas indicate no data (in this case near-shore regions).

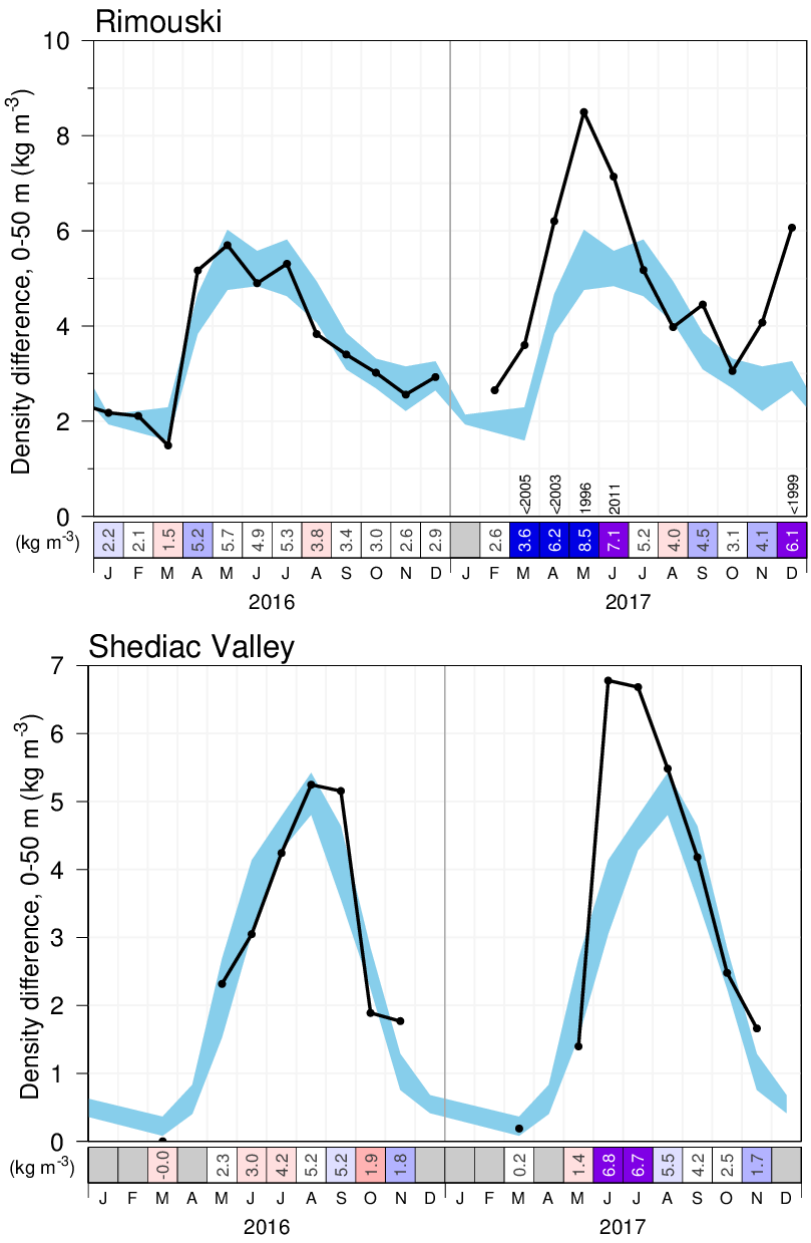

Figure 4. Seasonal stratification index (calculated as the density difference between 50 m and the surface) during 2016 and 2017 at Rimouski station (upper panel) and at Shediac Valley station (lower panel). The blue area represents the climatological monthly mean ± 0.5 SD (1991–2010 for Rimouski and 1981–2016 for Shediac Valley). The bottom scorecards have reverse colour codes: positive anomalies are shown in blue and correspond to low salinity and strong stratification. Numbers in the scorecard are the monthly density difference in kg m^{-3}. For anomalies greater than 2 SD from normal, the prior year with a greater anomaly is indicated.

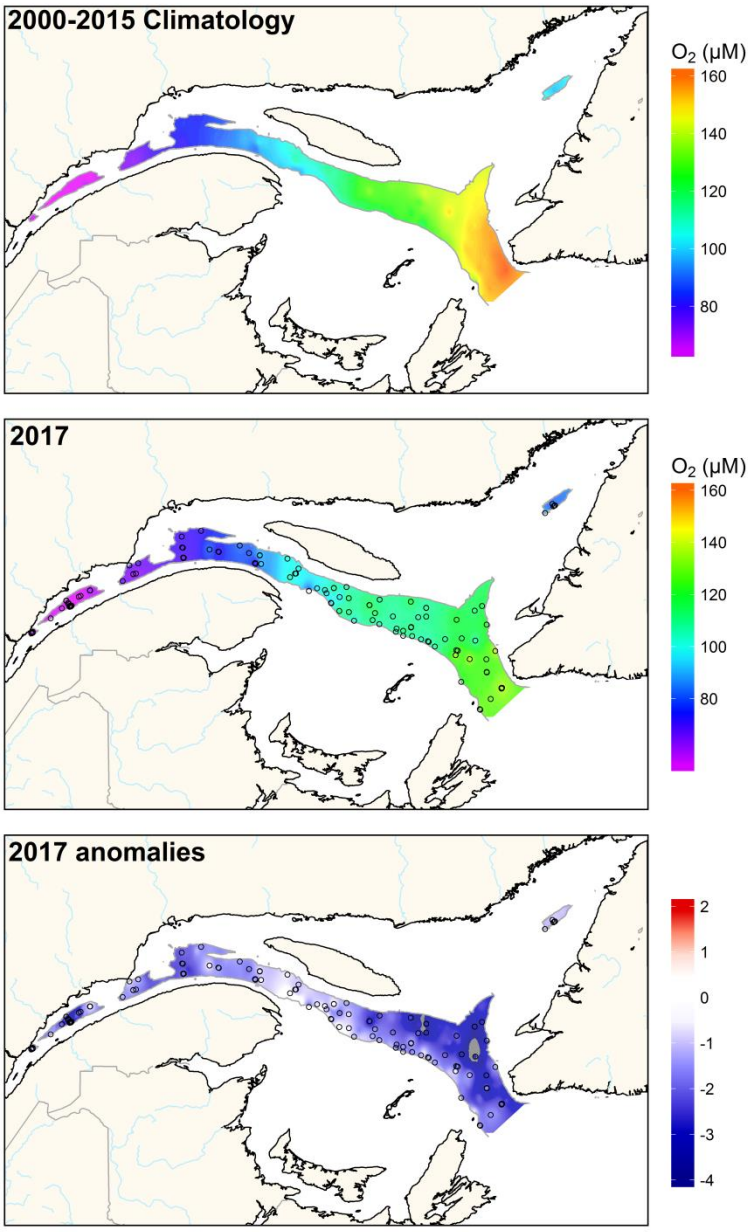

Figure 5. Annual average distribution of dissolved oxygen concentration at a depth of 300 m in the Estuary and Gulf of St. Lawrence during 2017 (upper panel). *The climatology (2000–2015; middle panel) and anomalies (lower panel) are also shown. Blue colours indicate anomalies below the mean and reds are anomalies above the mean.*

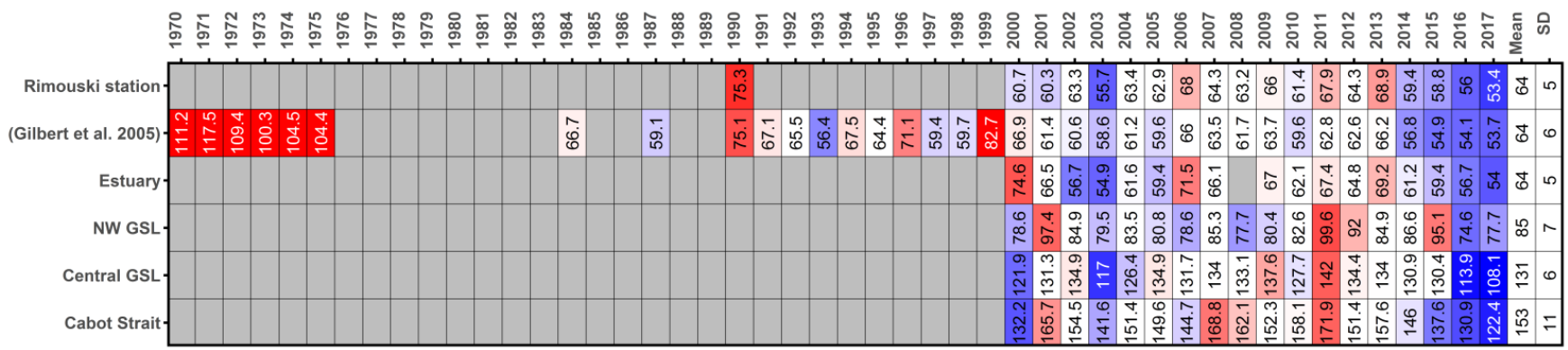

Figure 6. Time series of deep-layer dissolved oxygen concentration (µM). This figure updates the time series presented in Galbraith et al. (2017) and uses the same subregions. The time series associated with Gilbert et al. (2005) is for the Estuary. The numbers on the right are the 2000–2015 climatological means and standard deviations, and the numbers in the boxes are the oxygen concentrations. Cell colour represents the anomaly: blue colours indicate anomalies below the mean and reds are anomalies above the mean.

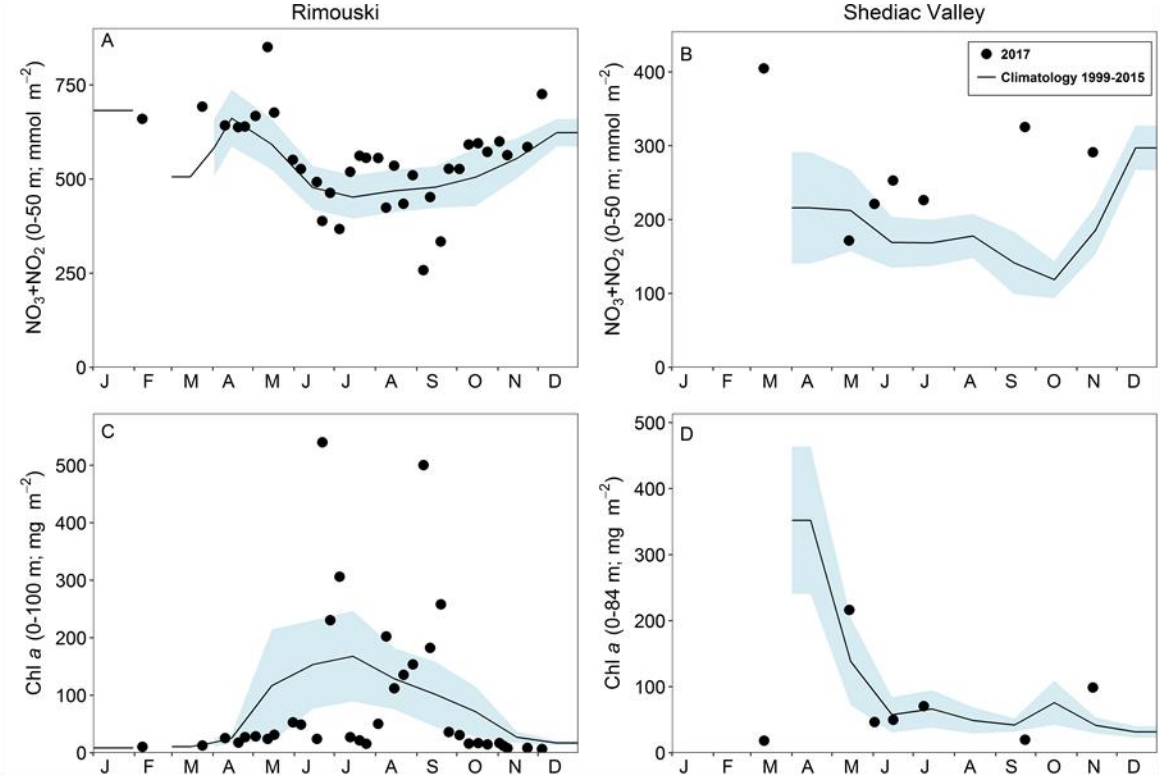

E

Rimouski

	1999	2000	2001	2002	2003	2004	2005	2006	2007	2008	2009	2010	2011	2012	2013	2014	2015	2016	2017	Mean	SD
Chl a 0-100m	1.83	-0.42	0.39	-0.28	0.42	-0.78	-0.57	-0.53	0.2	-0.79	-0.14	-0.19	-0.32	0.25	-0.23	0.85	0.02	1.98	-0.13	86.8	65.9
Nitrate 0-50m	0	0.46	-0.06	1.33	-0.24	0.71	-0.63	-0.03	-0.58	0.55	-0.36	-1.25	-0.5	-0.21	0.09	0.28	0.52	-0.8	0.28	539.1	90.4
Nitrate 50-150m	-0.32	-0.25	0.4	0.92	-0.47	-0.29	0.09	0.39	0.66	-0.35	0.2	-1.08	-0.7	0.08	-0.44	0.61	0.54	0.11	-0.2	1449	188.8
Nitrate 150-320m	1.29	-0.99	-1.39	0.66	0.11	0.35	1	1.38	0.47	-0.93	0.25	-0.88	-0.58	-0.58	-0.01	0.18	0.46	-1.37	-1.68	4036.1	123.2

Shediac Valley

	1999	2000	2001	2002	2003	2004	2005	2006	2007	2008	2009	2010	2011	2012	2013	2014	2015	2016	2017	Mean	SD
Chl a 0-100m	-0.46	-0.34	-0.13	1.48	0.17	-0.44	-0.42	0.08	0.41	0.6	-0.07	-0.28	-0.74	-0.14	0.33	-0.35	-0.41	-0.58	0.36	91.7	62
Nitrate 0-50m	0.29	0.56	-0.03	0.24	0.25	0.53	-0.64	0.32	-1.17	-0.2	0.52	-1.13	-0.09	0.09	0.06	0.7	-0.34	-0.09	1.32	187.9	72.1
Nitrate 50-84m	0.08	0.88	0.21	0.57	0.03	-0.2	-0.43	0.86	-1.17	0.13	0.07	-1.45	-0.96	-0.08	-0.14	0.64	0.05	0.07	0.29	290.6	62.3

Figure 7. Nitrate inventories (0–50 m; top panels) and chlorophyll a levels (0–100 m Rimouski and 0–84 m Shediac Valley; bottom panels) in 2017 (black circles) with monthly mean conditions (± 0.5 SD) for the 1999–2015 reference period (black line with blue shading) at Rimouski and Shediac Valley stations. Time series of normalized annual anomalies for nitrate inventories (mmol m^{-2}) and chlorophyll a levels (mg m^{-2}) are also presented with the variable means and standard deviations for the 1999–2015 reference period at the right end of the scorecard. Blue colours indicate anomalies below the mean and reds are anomalies above the mean.

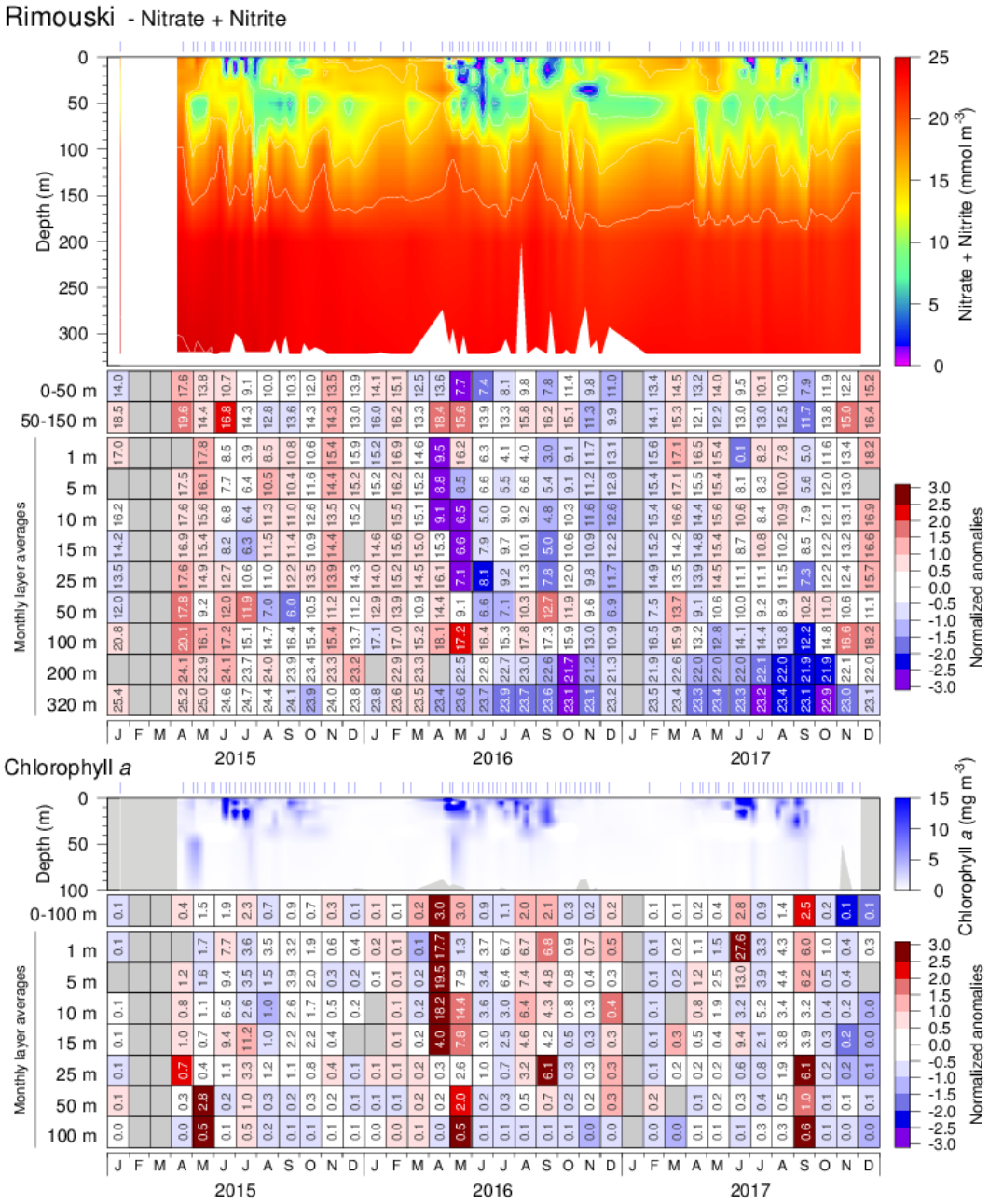

Figure 8. Nitrate (top) and chlorophyll a (bottom) concentrations at Rimouski station during the 2015 to 2017 sampling seasons. Contour plots are made with data from individual sorties while monthly means are shown in the tables below the graphics (nitrates: mmol m^{-3}; chl a: mg m^{-3}). Cell colours indicate normalized anomalies based on the 1991–2015 climatology: blue colours indicate anomalies below the mean and reds are anomalies above the mean. During March, the integrated (0–50) monthly average and the depth-specific average for nitrate for the reference period do not include the same amount of data, and this might result in inconsistent anomalies between integrated and depth-specific values.

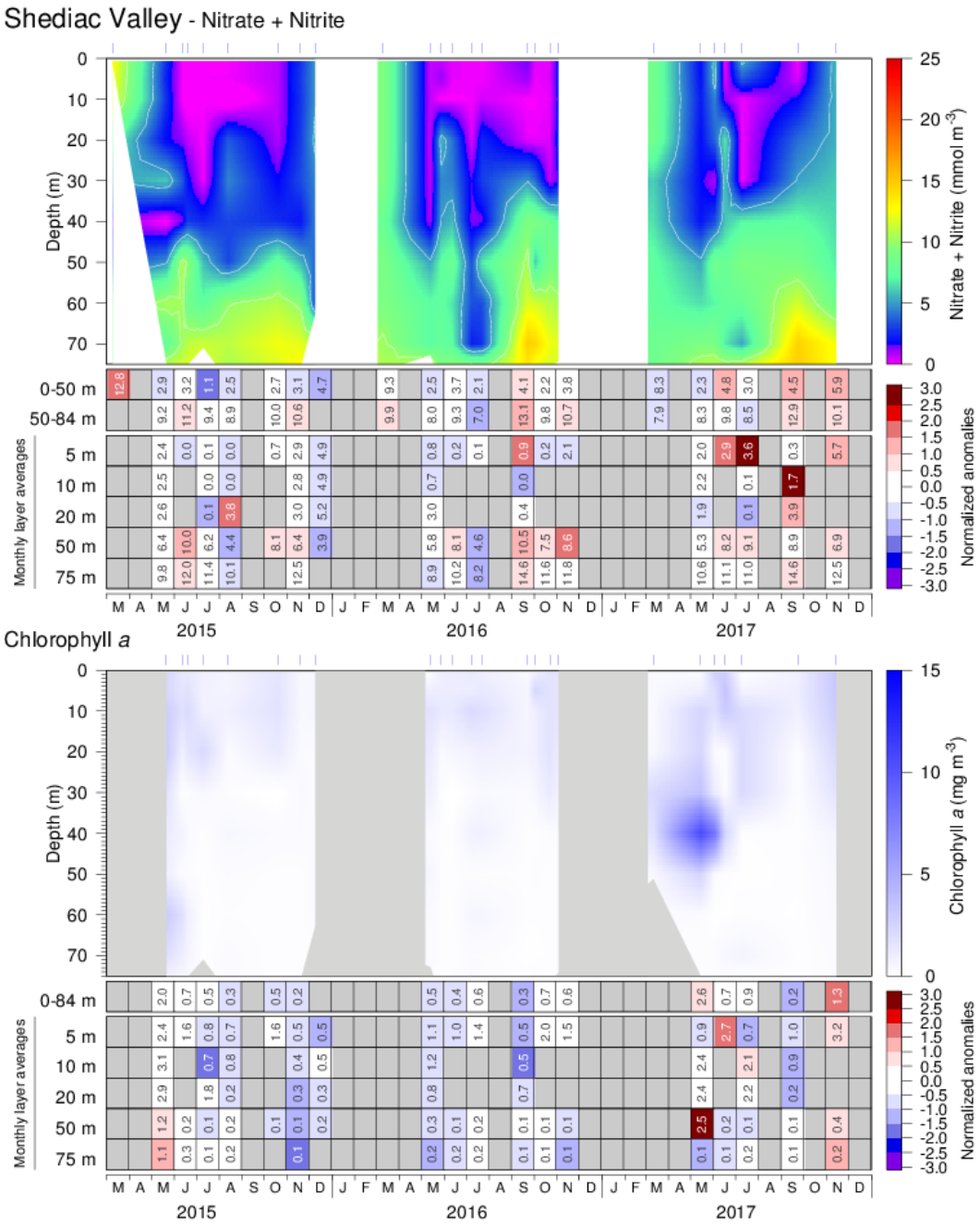

Figure 9. Nitrate (top) and chlorophyll a (bottom) concentrations at Shediac Valley station during the 2015 to 2017 sampling seasons. Contour plots are made with data from individual sorties while monthly means are shown in the tables below the graphics (nitrates: mmol m^{-3}; chl a: mg m^{-3}). Nitrate values in March are from the winter survey across the Gulf. Cell colours indicate normalized anomalies based on the 1991–2015 climatology: blue colours indicate anomalies below the mean and reds are anomalies above the mean. Only seven to ten observations per year were used to produce annual vertical profiles, so interpolation between sampling date (blue tick marks above vertical profiles) might not be accurate.

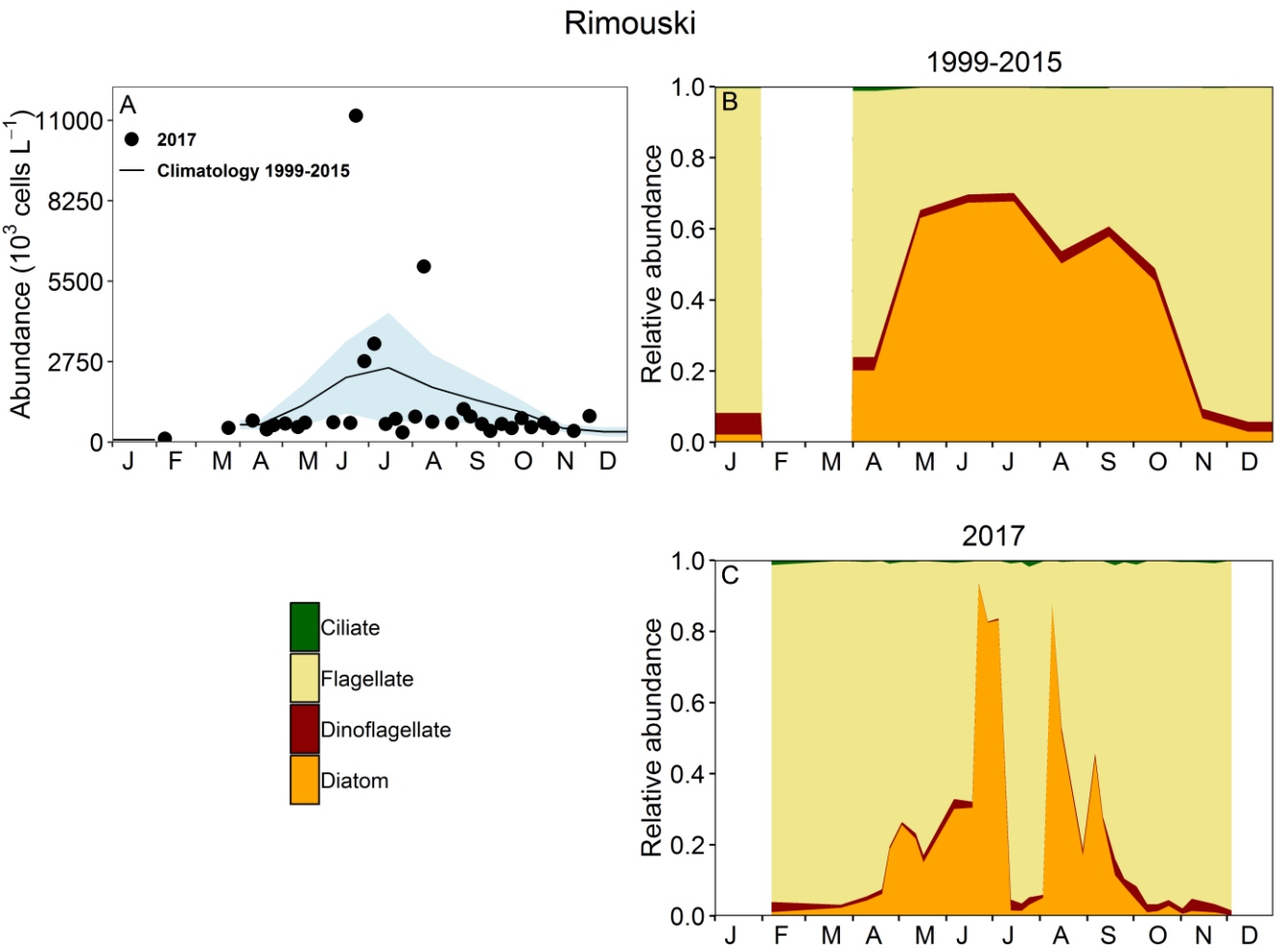

Figure 10. Phytoplankton abundance (A) and community composition at Rimouski station for the 1999–2015 reference period (B; no data in 2010) and for 2017 (C). Blue shading on panel (A) represents ± 0.5 SD of the monthly mean phytoplankton abundance for the reference period.

Rimouski

	1999	2000	2001	2002	2003	2004	2005	2006	2007	2008	2009	2010	2011	2012	2013	2014	2015	2016	2017	Mean	SD
Diatom	0.15	0.2	0.45	0.17	0.33	-0.71	-0.47	-0.32	0.18	-0.53	0.47		0.14	0.01	-0.46	0.29	0.39	3.9	-0.29	807	892
Dino	-0.37	-0.56	-0.12	0.26	0.34	-0.05	0.32	1.17	1.44	-0.03	0.62		-0.24	-0.15	-0.55	-0.86	-0.96	-0.94	-1.1	40	25
Flag	-0.87	-0.97	-0.55	-0.67	-0.11	-0.63	0.82	1.4	1.34	0.14	0.97		-0.35	-0.5	0.09	-0.24	0.35	0.79	0.12	572	334
Ciliate	-0.94	-0.97	0.15	0.3	0.17	-1.01	1.23	0.76	0.52	-0.28	-0.14		0.02	0.65	-0.15	-0.13	-0.28	-0.42	-0.58	6	4
Total	-0.14	-0.11	0.31	-0.03	0.34	-0.89	-0.13	0.42	0.55	-0.43	0.67		-0.02	-0.18	-0.39	0.05	0.37	2.97	-0.03	1426	1036
Diat/Dino	1.21	0.33	0.35	-0.07	-0.16	-0.69	-0.59	-0.61	-0.43	-0.57	-0.14		0.22	0.02	-0.32	0.77	0.56	7.04	0.9	29	45
Diat/Flag	1.23	0.67	0.48	0.31	0.19	-0.63	-0.6	-0.53	-0.3	-0.63	-0.2		0.14	0.15	-0.45	0.22	-0.05	0.94	-0.38	2	2

Shediac Valley

	1999	2000	2001	2002	2003	2004	2005	2006	2007	2008	2009	2010	2011	2012	2013	2014	2015	2016	2017	Mean	SD
Diatom	-0.51	0.19	-0.25	1.07	0.03	-0.02	-0.3	-0.2	1.21	0.36	-0.24	-0.54	-0.51	-0.3	0.15	-0.64	-0.48	-0.61	0.27	171	226
Dino	0.36	1.31	0.06	0.28	-0.19	0.99	0.16	-0.75	-0.45	0.86	-0.77	-0.62	-0.34	-0.5	-0.68	-0.08	0.11	1.62	0.63	5	4
Flag	-0.72	-0.02	0.63	0.67	0.34	0.41	0.15	-0.21	-0.53	0.22	-0.58	-0.69	0.8	-0.5	-0.39	1.02	-0.49	3.3	1.52	21	23
Ciliate	0.96	0.31	-0.3	0.3	-0.3	0.56	-0.33	-0.76	0.02	0.33	-0.08	-0.43	0.36	-0.37	-0.14	-0.01	0.18	1.15	1.08	1	1
Total	-0.57	0.2	-0.2	1.14	0.07	0.19	-0.32	-0.34	1.16	0.43	-0.33	-0.65	-0.21	-0.4	-0.05	-0.4	-0.48	-0.21	0.78	198	232
Diat/Dino	-0.64	-0.47	-0.13	0.69	0.1	-0.28	-0.29	0.17	1.3	0.12	0.13	-0.14	-0.31	-0.21	0.32	-0.66	-0.51	-0.66	-0.24	50	62
Diat/Flag	-0.31	-0.46	-0.34	0.29	0.64	-0.41	-0.26	0.31	1.33	0.04	0.01	-0.24	-0.51	-0.13	-0.05	-0.6	0.05	-0.57	-0.48	51	56
	1999	2000	2001	2002	2003	2004	2005	2006	2007	2008	2009	2010	2011	2012	2013	2014	2015	2016	2017	Mean	SD

Figure 11. Time series of normalized annual (April–November) anomalies for abundance (10^3 cells L^{-1}) of the main phytoplankton taxonomic groups (diatoms, dinoflagellates, flagellates, ciliates) and total microphytoplankton, and for the diatom/dinoflagellate and diatom/flagellate ratios at Rimouski and Shediac Valley stations. Variable means and standard deviations for the1999–2015 reference period are shown at the right end of the scorecard. Blue colours indicate anomalies below the mean and reds are anomalies above the mean. No data are available for 2010 at Rimouski station.

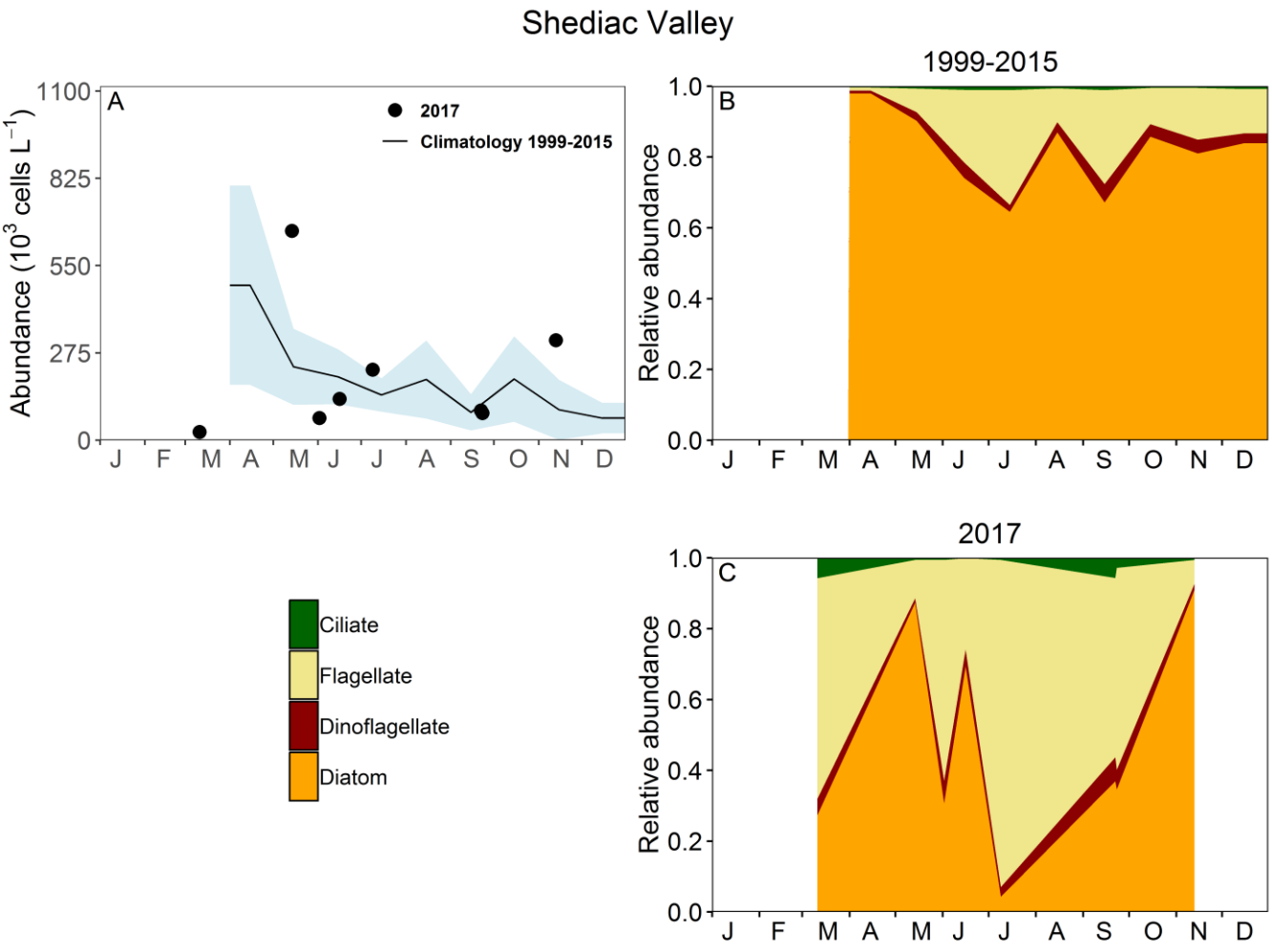

Figure 12. Phytoplankton abundance (A) and community composition at Shediac Valley station for the 1999–2015 reference period (B) and for 2017 (C). Blue shading on panel (A) represents ± 0.5 SD of the monthly mean phytoplankton abundance for the reference period.

NO_3+NO_2 (0-50 m; mmol m^{-2})

		1999	2000	2001	2002	2003	2004	2005	2006	2007	2008	2009	2010	2011	2012	2013	2014	2015	2016	2017	Mean	SD
Winter	wGSL	1.73	-0.42	0.26	0.3	1.58	0.32	-0.46	0.37	1.48	-0.43	0.19	-1.51	-1.8	-0.29	0.38	-0.6	-1.1	0.19	-1.17	563.6	92
	eGSL			-0.04	0.13	1.94	1.02	-0.83	-0.16	0.96	-0.29	-0.14	-2.47	-0.72	-0.57	0.41	0.48	0.28	-1.28	-0.21	301.9	46
	sGSL	0.11	1.49	-0.18	1.01	0.93	1.06	-0.57	0.66	0.18	-0.59	0.24	-2.27	-0.98	-1.54	-0.66	0.41	0.7	-0.24	-0.32	367.6	95
Summer	wGSL	-1.46	-0.45	0.4	1.12	-0.07	0.6	-1.09	0.02	-0.19	0.35	-1.1	-1.06	-1.06	-0.51	1.64	1.65	1.2	-0.85	0.15	315.8	57.6
	eGSL	-0.79	0.51	-0.22	-1.2	1.85	-1.24	-0.5	0.18	0.92	1.4	-0.21	-0.53	-1.18	-0.9	-0.28	1.62	0.59	-1.37	-1.37	66.7	23
	sGSL	-0.32	0.37	-1.14	0.19	0.53	-0.13	-0.26	1.94	-0.11	1.15	1.1	-2.09	-0.65	-0.98	0.88	0.49	-0.98	-1.37	-0.49	110.5	32.4
W - S	wGSL	2.24	-0.11	0.01	-0.34	1.38	-0.05	0.19	0.3	1.35	-0.55	0.74	-0.72	-0.96	0.02	-0.55	-1.39	-1.57	0.62	-1.07	247.8	108.6
	eGSL			0.1	0.68	1.17	1.87	-0.63	-0.27	0.59	-1.09	-0.01	-2.46	-0.12	-0.11	0.65	-0.36	0	-0.65	0.56	234.2	40.8
	sGSL	0.26	1.57	0.24	0.94	0.87	1.28	-0.55	0	0.26	-1.12	-0.15	-1.77	-0.86	-1.37	-1.09	0.29	1.19	0.26	-0.16	256.4	82.7
Fall	wGSL	1.63	-0.61	-0.11	1.64	-0.38	-1.52	-0.69	-0.52	-1.1	-0.74	-0.74	0.72	-0.41	1.51	0.13	-0.15	1.33	0.28	0.2	359.2	69.4
	eGSL	1.77	1.35	-0.8	1.74	0.46	-1.09	-0.08	-0.36	1.05	0.03	0.38	-0.37	-1.44	-1.06	-0.18	-1.04	-0.37	-1.28	0.43	115.1	24.4
	sGSL	1.12	0.37	-1.18	-0.24	-0.15	1.83	0.44	2.12	-0.82	0.3	-0.23	-0.67	-0.93	-0.36	0.06	0.03	-1.69	-1.08	0.56	170	35.5

NO_3+NO_2 (Summer & Fall; mmol m^{-2} or mmol m^{-3})

		1999	2000	2001	2002	2003	2004	2005	2006	2007	2008	2009	2010	2011	2012	2013	2014	2015	2016	2017	Mean	SD
0-50 m	wGSL	0.09	-0.53	0.14	1.38	-0.22	-0.46	-0.89	-0.25	-0.64	-0.2	-0.92	-0.17	-0.73	0.5	0.88	0.75	1.26	-0.29	0.18	337.5	63.5
	eGSL	0.49	0.93	-0.51	0.27	1.15	-1.17	-0.29	-0.09	0.98	0.71	0.08	-0.45	-1.31	-0.98	-0.23	0.29	0.11	-1.33	-0.47	90.9	23.7
	sGSL	0.4	0.37	-1.16	-0.03	0.19	0.85	0.09	2.03	-0.46	0.72	0.44	-1.38	-0.79	-0.67	0.47	0.26	-1.33	-1.22	0.03	140.3	33.9
50-150 m	wGSL	0.19	-1.14	0.63	0.68	0.37	-1.25	-0.62	0.56	-0.02	0.13	-0.28	-1.08	-0.99	0.69	0	0.32	1.82	-0.02	0.06	1366.4	143.7
	eGSL	-0.6	0.79	-1.59	-0.23	0.21	-1.61	-0.77	1.18	-0.7	0.22	0.28	-0.14	-0.38	0.48	0.43	0.54	1.88	-0.27	-1.44	879.2	99.9
	sGSL																					
300m	wGSL	-1.85	-1.8	-0.61	0.39	0.23	-0.35	0.09	1.07	0.03	0.15	0.2	-0.12	-0.21	0.3	0.9	0.83	0.77	-0.24	-0.35	23.8	1.2
	eGSL	-1.65	-0.11	-0.58	-0.97	0.82	-0.5	-0.45	0.54	-0.92	0.03	-0.35	-0.1	0.37	0.92	1.22	0.48	1.24	1.23	1.19	22.2	1.1
	sGSL																					

Chl *a* (0-100 m; mg m^{-2})

		1999	2000	2001	2002	2003	2004	2005	2006	2007	2008	2009	2010	2011	2012	2013	2014	2015	2016	2017	Mean	SD
Summer	wGSL	1.39	-0.82	-0.09	0.75	2.07	-0.55	-1.22	-0.47	0.82	-1.3	0.9	0.24	-0.23	0.31	-1.71	0.31	-0.4	-0.81	-0.75	110.2	47
	eGSL	-0.37	0.09	-0.6	3.23	-0.83	-0.4	-0.6	-0.3	-0.2	0.19	-0.34	-0.14	-0.55	-0.58	-0.14	-0.16	1.7	-0.3	1.06	36.8	17.7
	sGSL	-0.33	-1.11	0.04	3.52	0.08	-0.28	-0.76	0.31	-0.04	-0.69	0.1	0.52	-0.69	-0.33	0.1	-0.41	-0.01	-0.17	1.87	37.3	14.3
Fall	wGSL	-0.35	-0.64	-0.14	-0.26	0.5	-0.4	0.24	-0.3	-0.31	3.59	-0.54	-0.69	-0.72	-0.14	-0.54	0.36	0.33	-0.71	-0.98	35.9	18
	eGSL	-0.51	-0.5	-0.82	1.97	0.62	-0.48	-1.09	-1.09	0.28	-0.58	0.7	-0.2	-0.77	-0.89	0.17	1.13	2.07	1.54	-0.77	37.3	6.9
	sGSL	-0.54	-1.77	0.13	2.61	0.46	-1.01	-1.11	-0.89	1.06	-0.26	-0.4	-0.17	-0.05	0.58	0.75	0.33	0.28	0.14	2.06	40.7	16
S & F	wGSL	0.52	-0.73	-0.11	0.25	1.28	-0.47	-0.49	-0.38	0.25	1.15	0.18	-0.23	-0.48	0.09	-1.12	0.34	-0.04	-0.76	-0.87	73.1	32.5
	eGSL	-0.44	-0.2	-0.71	2.6	-0.1	-0.44	-0.85	-0.69	0.04	-0.2	0.18	-0.17	-0.66	-0.74	0.02	0.49	1.89	0.62	0.15	37.1	12.3
	sGSL	-0.43	-1.44	0.08	3.07	0.27	-0.65	-0.93	-0.29	0.51	-0.48	-0.15	0.17	-0.37	0.13	0.42	-0.04	0.14	-0.02	1.97	39	15.2

Figure 13. Time series of normalized seasonal anomalies for nitrate inventories (mmol m^{-2}; top panel) and chlorophyll a levels (mg m^{-2}; bottom panel) over the GSL subregions. Time series of normalized anomalies for nitrate inventories averaged for summer and fall are also shown (middle panel) for different water column layers (mmol m^{-2}) or 300 m (mmol m^{-3}). Variable means and standard deviations for the 1999–2015 reference period are shown to the right of the scorecard. W–S is the difference in the nitrate inventory between winter and summer; S and F is the average anomaly for summer and fall. Blue colours indicate anomalies below the mean and reds are anomalies above the mean.

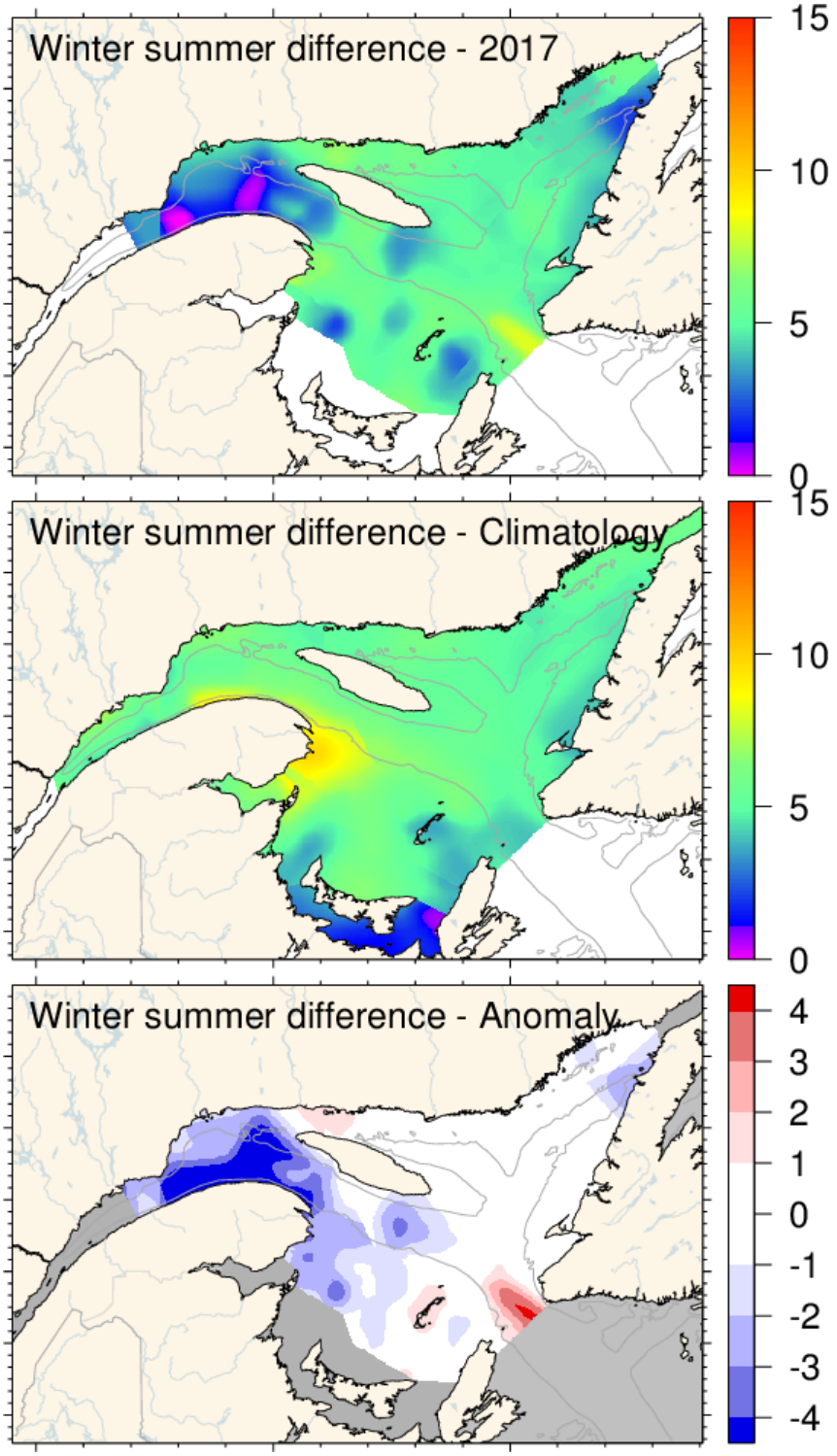

Figure 14. Difference in total nitrate (NO_3^- + NO_2^-) concentrations (mmol m^{-3}) at 2 m in the Estuary and Gulf of St. Lawrence between winter and summer. Top: winter–summer difference in 2017; middle: winter–summer climatology difference (2001–2015); bottom: winter–summer anomaly difference in 2017. Negative anomalies (blue) suggest weak nitrate drawdowns and positive anomalies (red) suggest strong nitrate drawdowns.

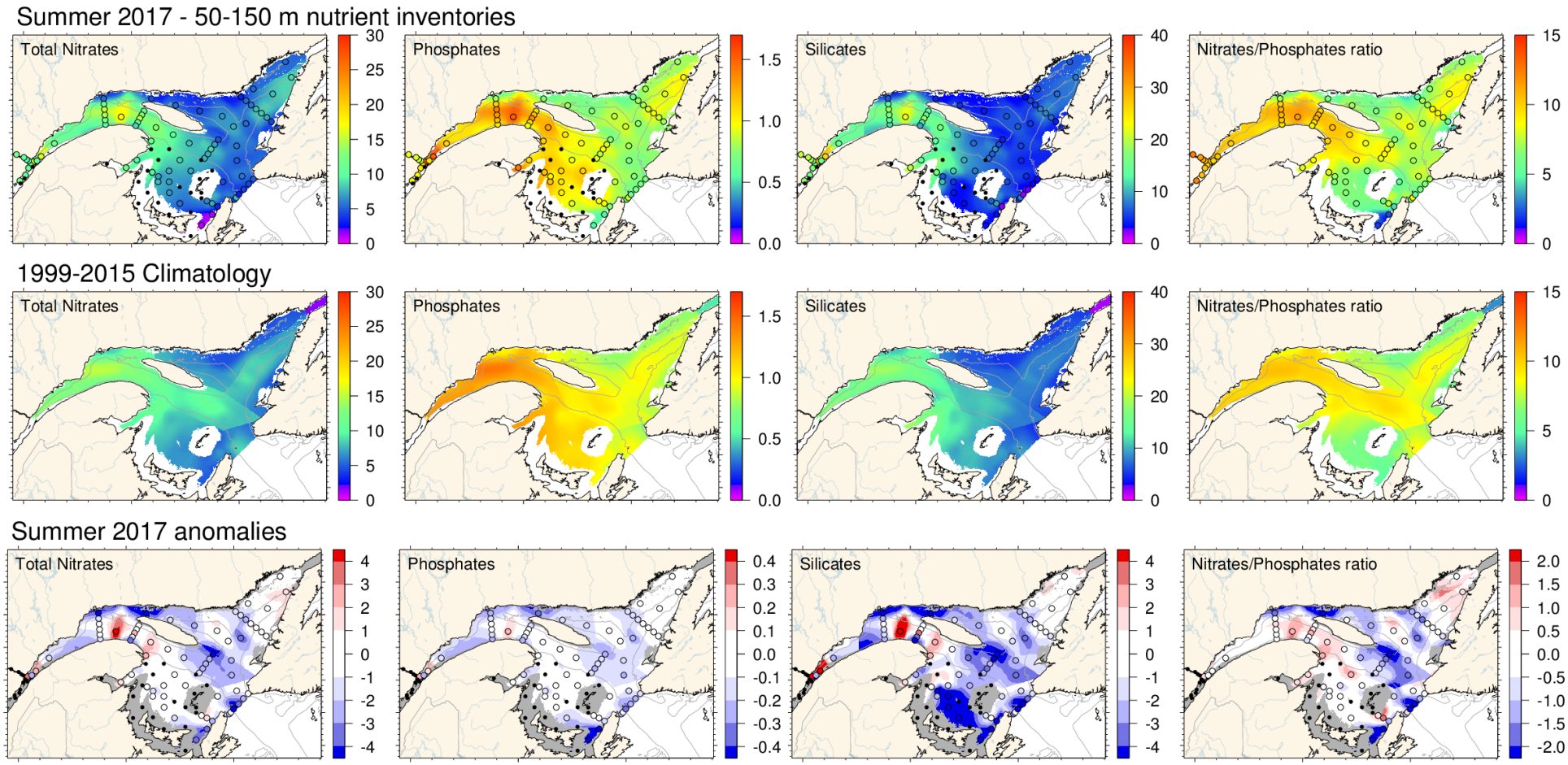

Figure 15. Total nitrate (NO_3^- + NO_2^-), phosphate, and silicate concentrations (mmol m^{-3}) and N:P ratio averaged over the mid-layer (50–150 m) in the Estuary and Gulf of St. Lawrence during June 2017 (upper panels). The climatology (1999–2015; middle panels) and anomalies (lower panels) are shown for each nutrient. Blue colours indicate anomalies below the mean and reds are anomalies above the mean.

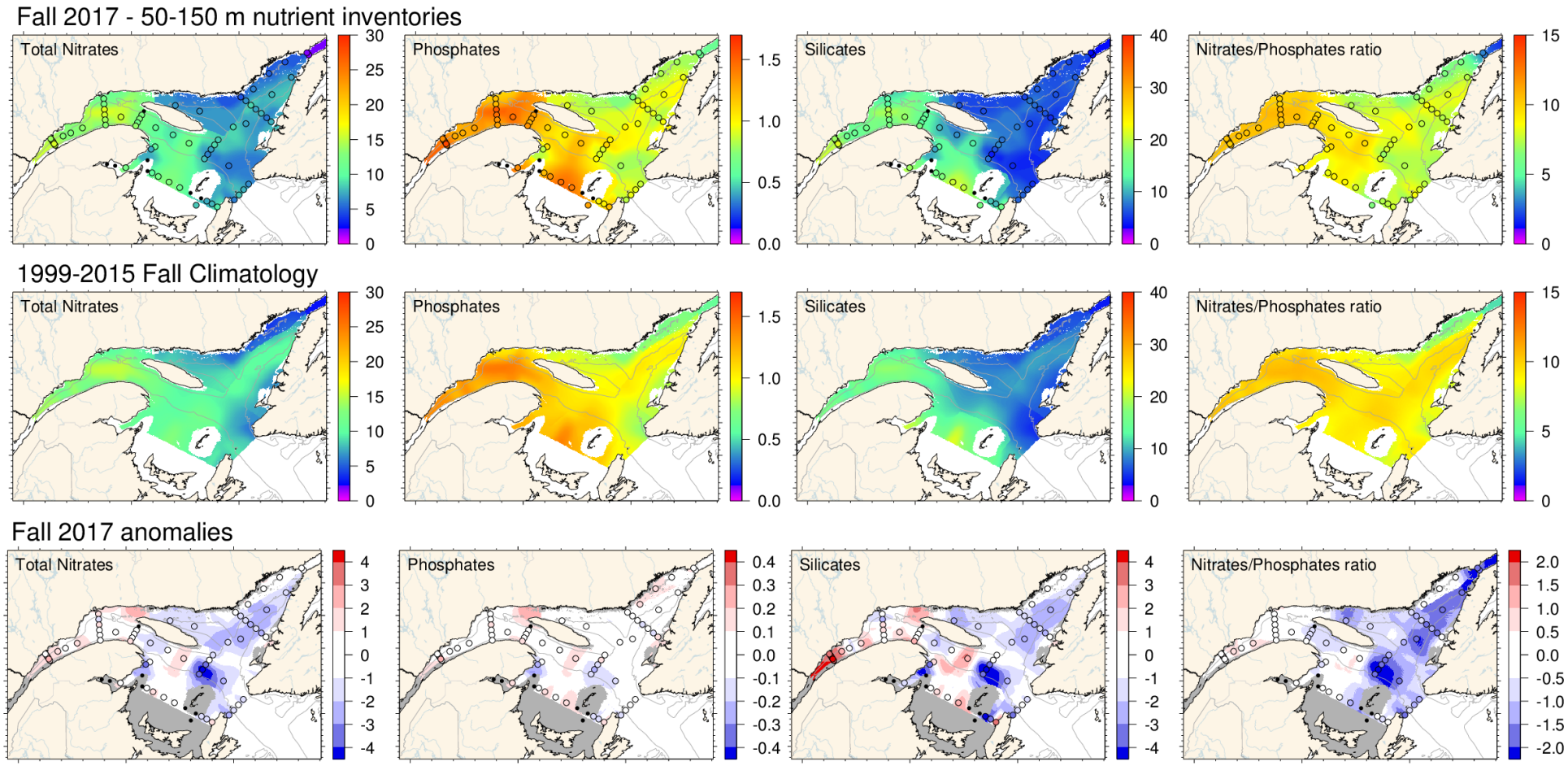

Figure 16. Total nitrate (NO_3^- + NO_2^-), phosphate, and silicate concentrations (mmol m^{-3}) and N:P ratio averaged in the mid-layer (50–150 m) in the Estuary and Gulf of St. Lawrence during November 2017 (upper panels). The climatology (1999–2015; middle panels) and anomalies (lower panels) are shown for each nutrient. Blue colours indicate anomalies below the mean and reds are anomalies above the mean.

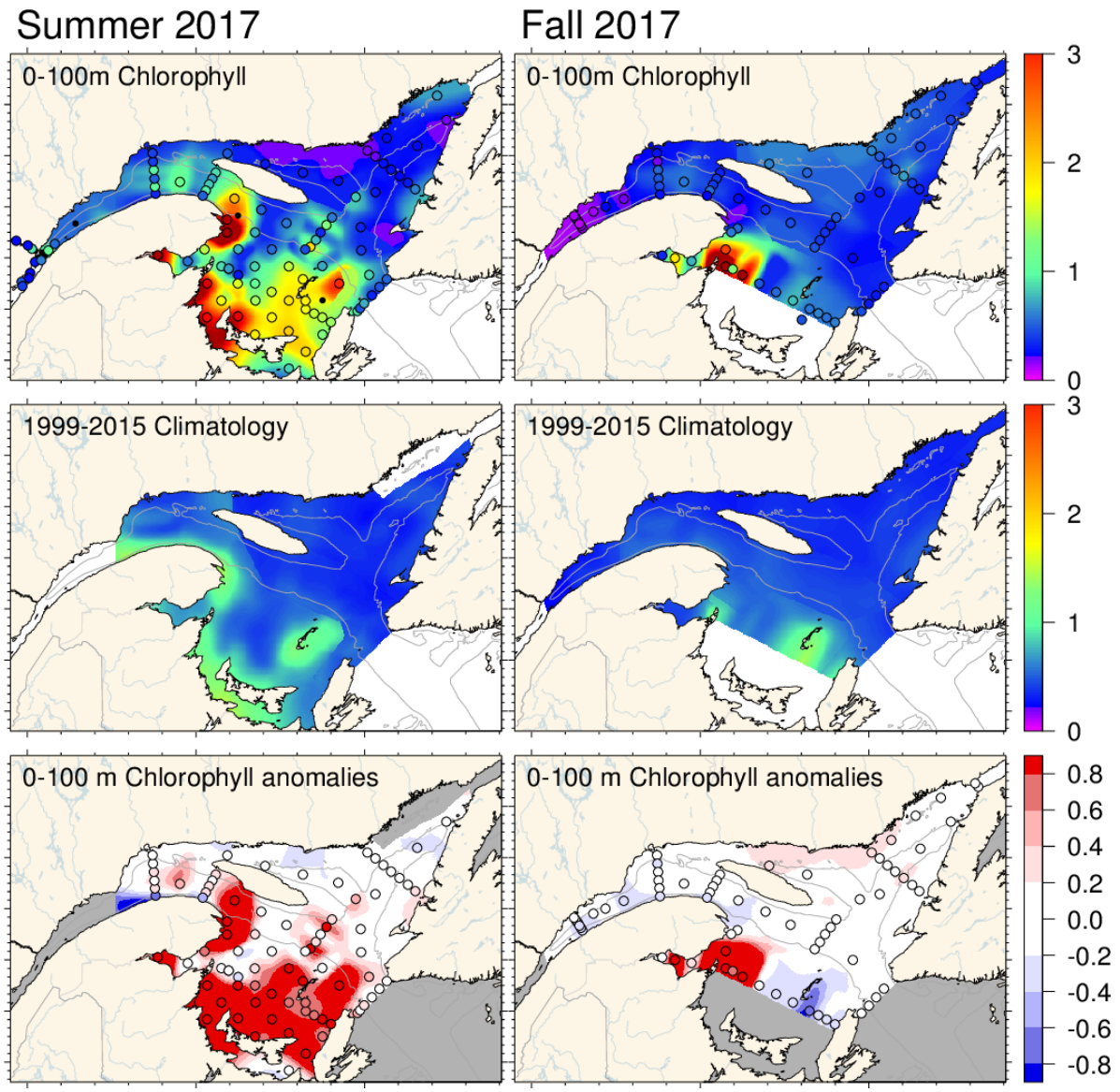

Figure 17. Vertically averaged (0–100 m) chlorophyll a concentrations (mg m^{-3}) in the Estuary and Gulf of St. Lawrence during summer (left panels) and fall (right panels) 2017. The climatology (1999–2015; middle panels) and anomalies (lower panels) are shown for both periods. Blue colours indicate anomalies below the mean and reds are anomalies above the mean.

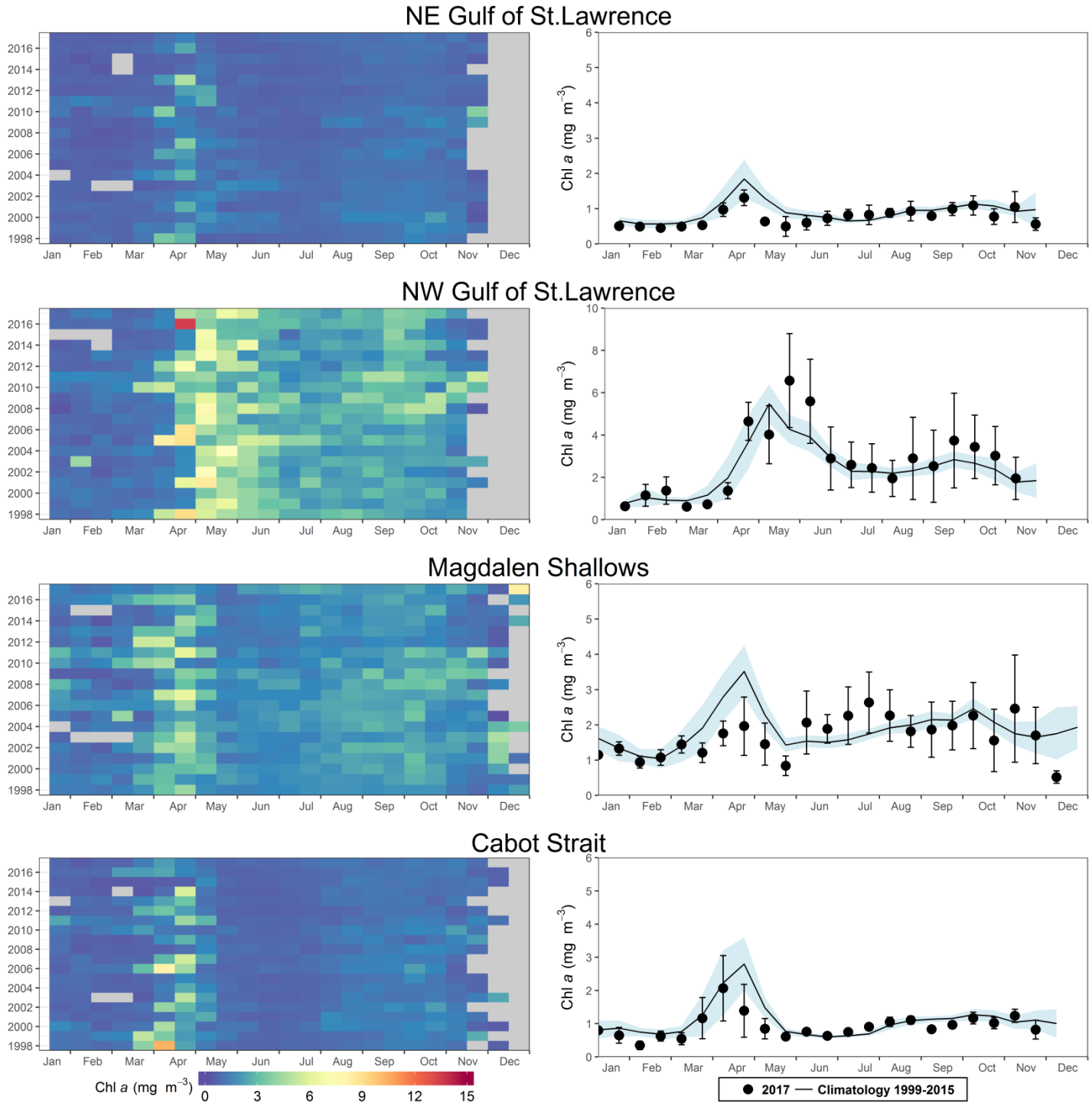

Figure 18. Left panels: Time series of surface chlorophyll a concentrations from twice-monthly SeaWiFS (1998–2007), MODIS (2008–2011), and VIIRS (since 2012) ocean colour data in the northeast Gulf of St. Lawrence, northwest Gulf of St. Lawrence, Magdalen Shallows, and Cabot Strait statistical subregions (see Fig. 3). Right panels: comparison of mean 2017 (black circles) surface chlorophyll a estimates using satellite ocean colour data with mean (± 0.5 SD) conditions from 1999–2015 (solid line with blue shading) for the same statistical subregions.

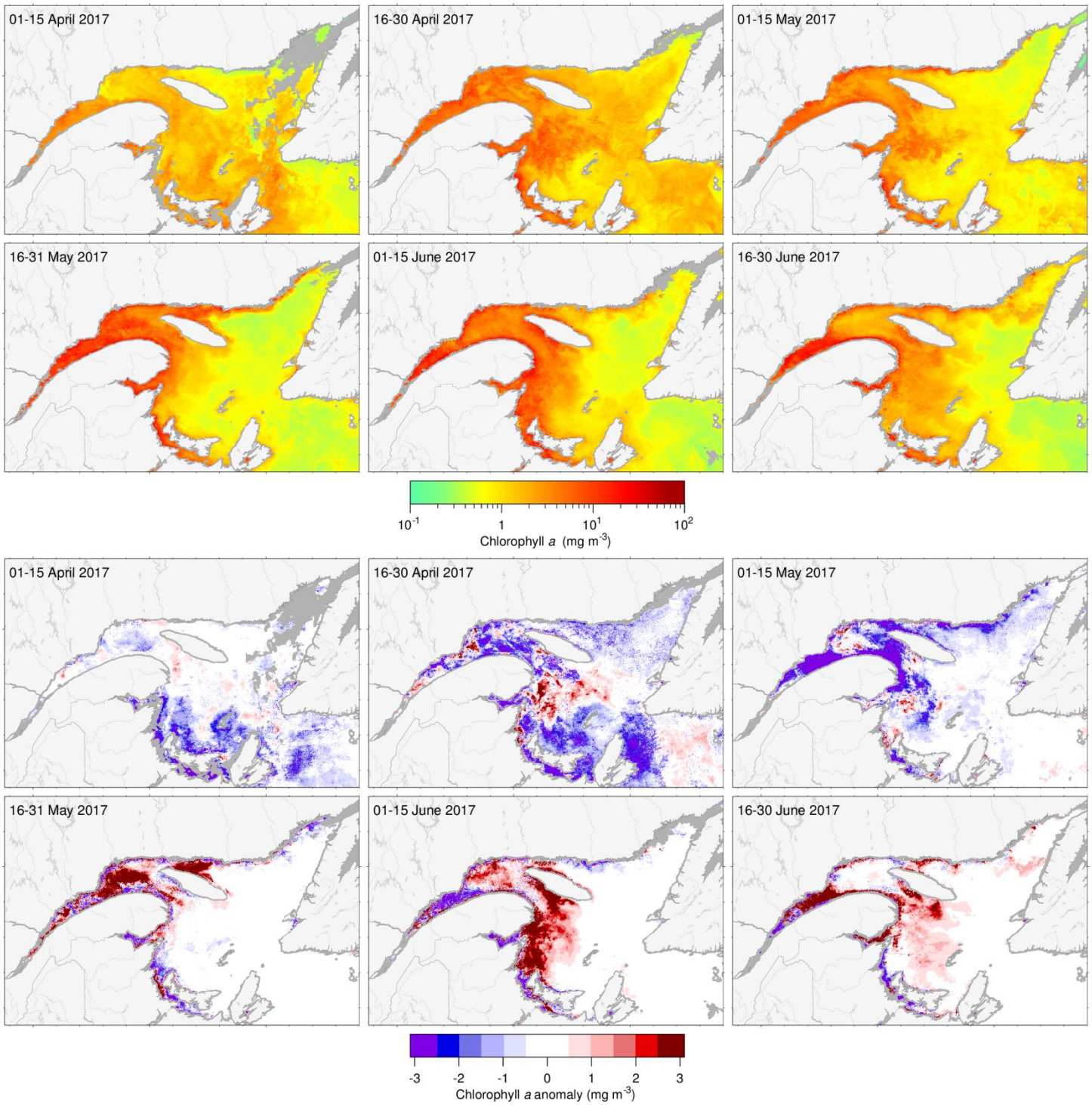

Figure 19. VIIRS twice-monthly composite images of surface chlorophyll a *(upper panels) and anomaly based on the 1999–2015 climatology (lower panels) in the Gulf of St. Lawrence during spring/summer 2017.*

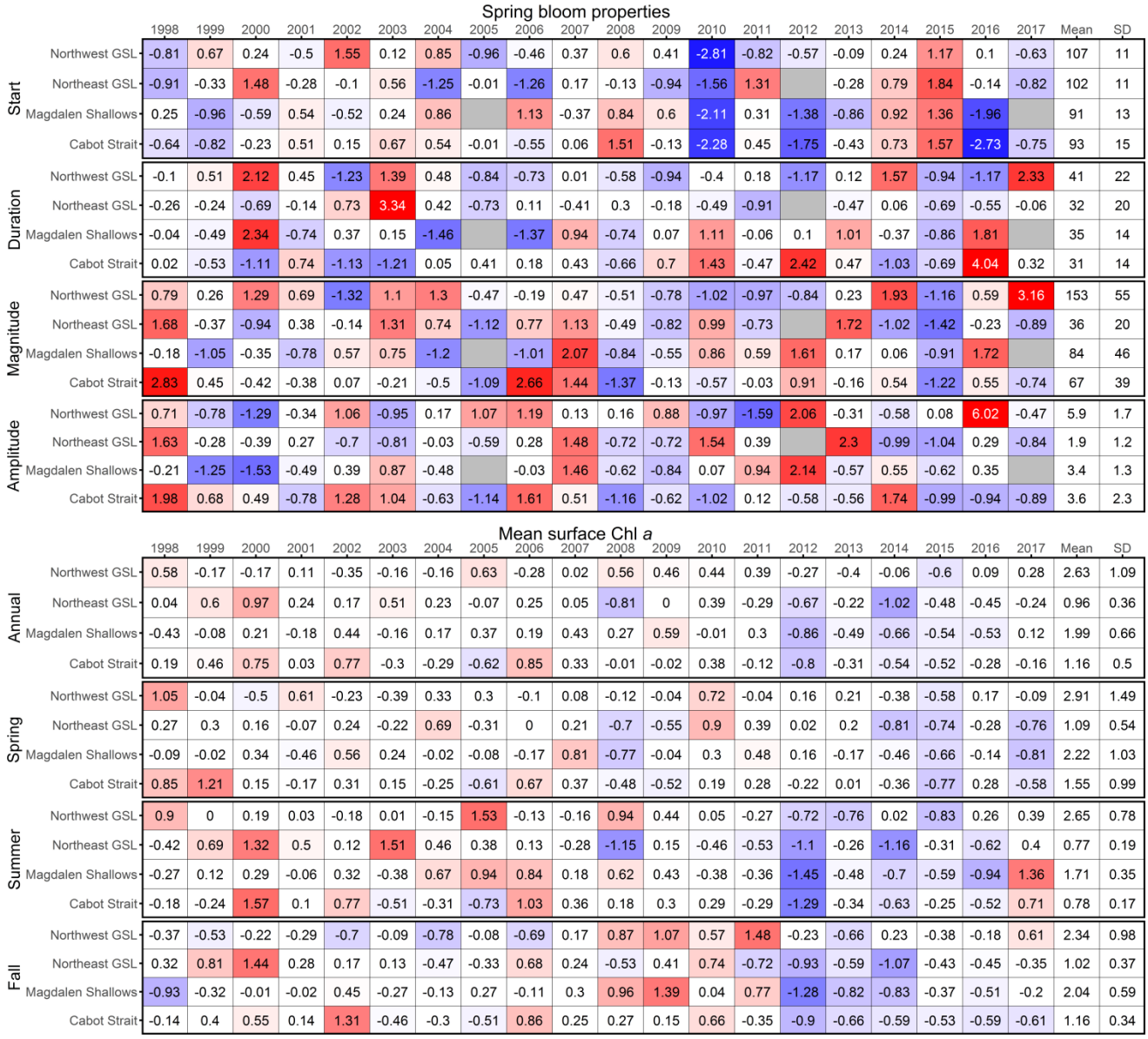

Figure 20. Time series of normalized anomalies for indices of change in spring bloom properties (upper section) and annual/seasonal mean surface chlorophyll a (lower section; mg m^{-3}) estimated from satellite ocean colour data (SeaWiFS, 1998–2007; MODIS, 2008–2011; and VIIRS since 2012) across the Gulf of St. Lawrence statistical subregions (see Fig. 3). The spring bloom indices are start (day of the year), duration (days), magnitude (mg chl m^{-2}), and amplitude (mg chl m^{-3}). The spring bloom was likely too small in the Magdalen Shallows during 2017 to calculate spring bloom parameters. Variable means and standard deviations for the 1999–2015 reference period are shown at the right end of the scorecard. Blue colours indicate anomalies below the mean and reds are anomalies above the mean. Spring is from March to May; summer is from June to August; fall is from September to November.

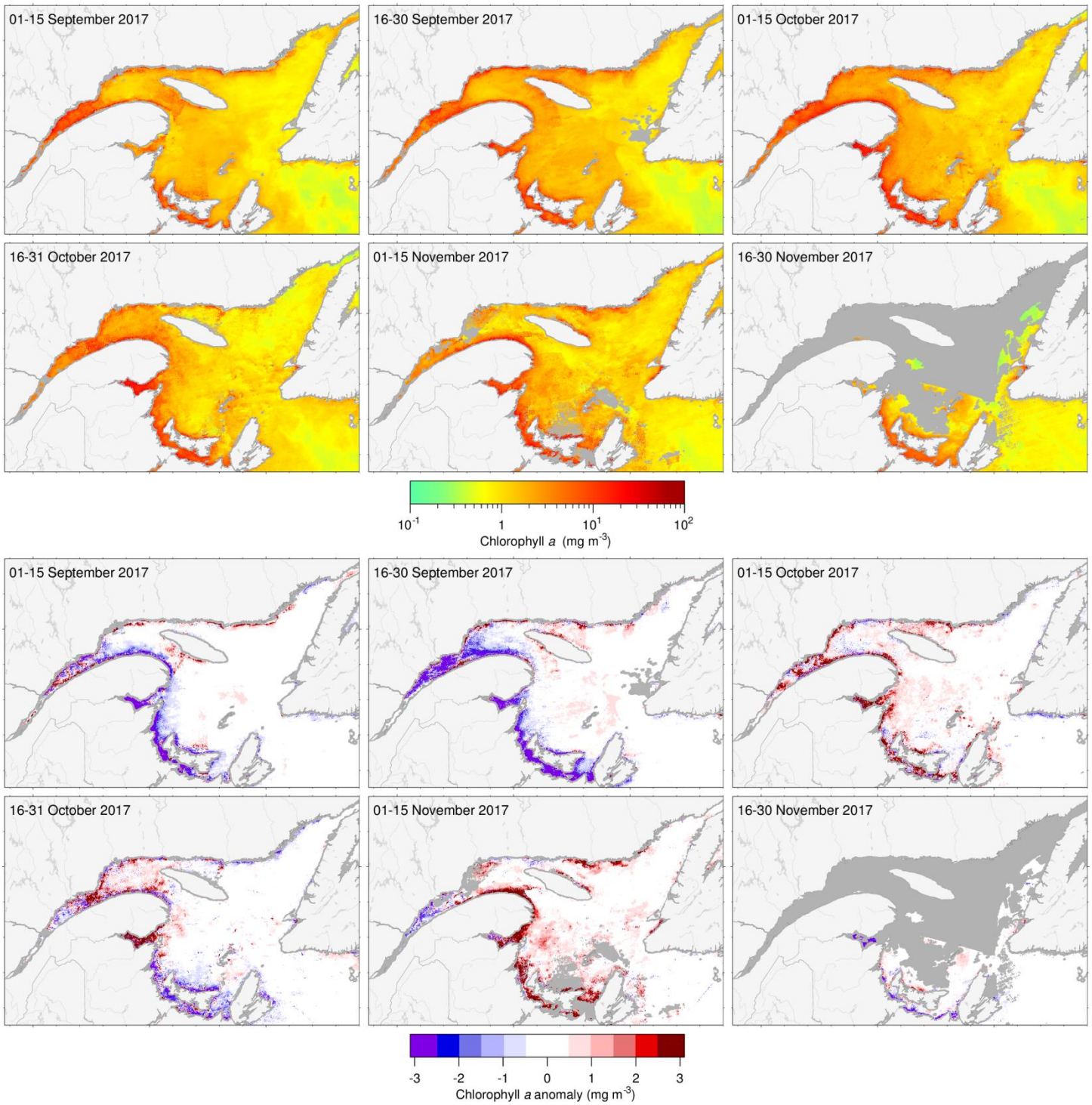

Figure 21. VIIRS twice-monthly composite images of surface chlorophyll a *(upper panels) and chlorophyll* a *anomaly based on the 1999–2015 climatology (lower panels) in the Gulf of St. Lawrence during fall 2017.*

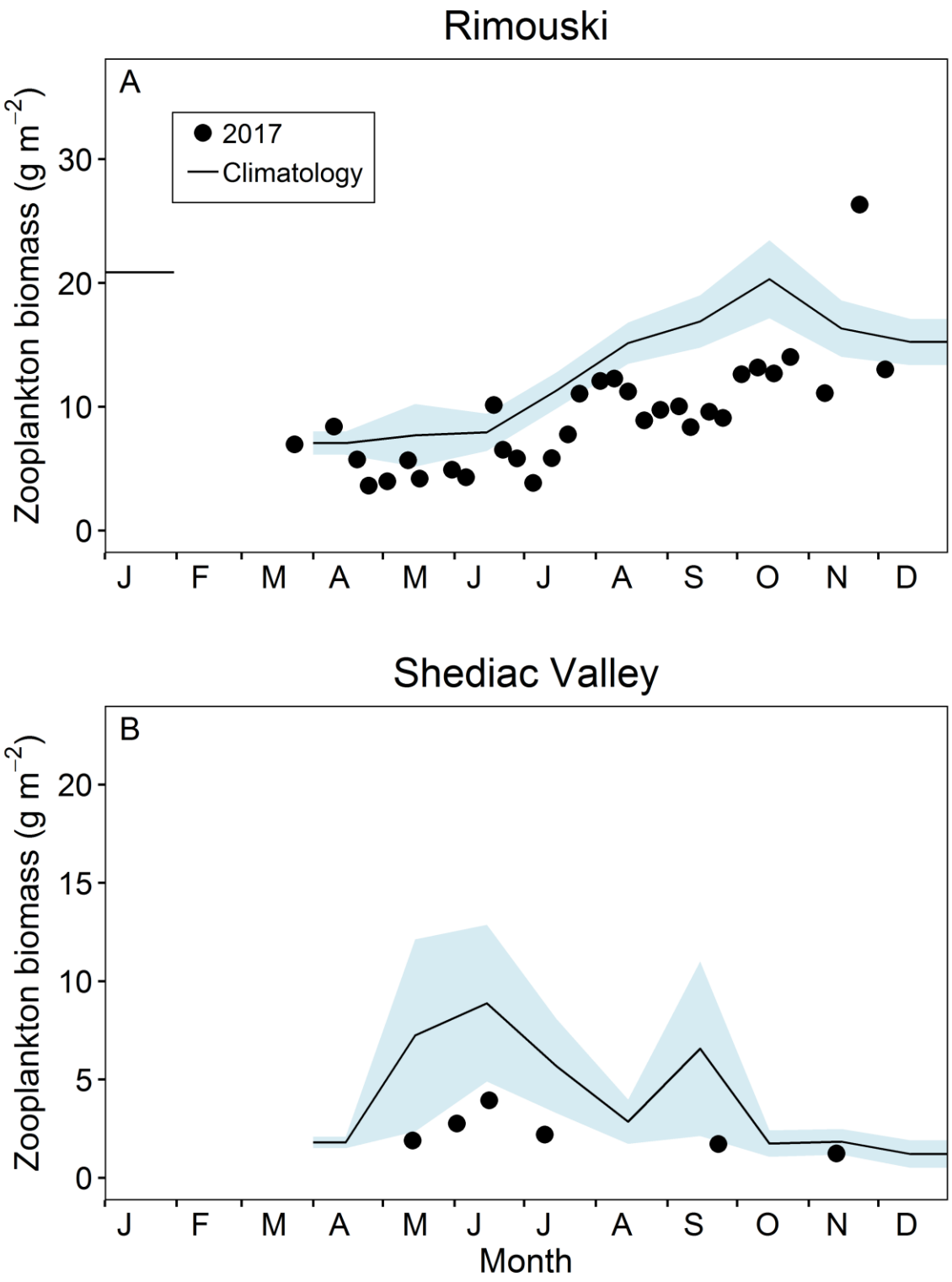

Figure 22. Comparison of total zooplankton biomass (dry weight) in 2017 (circles) with the monthly climatology from (A) Rimouski (2005–2015) and (B) Shediac Valley (1999–2015) stations (black line with blue shading). Blue shading represents 0.5 SD of the monthly means.

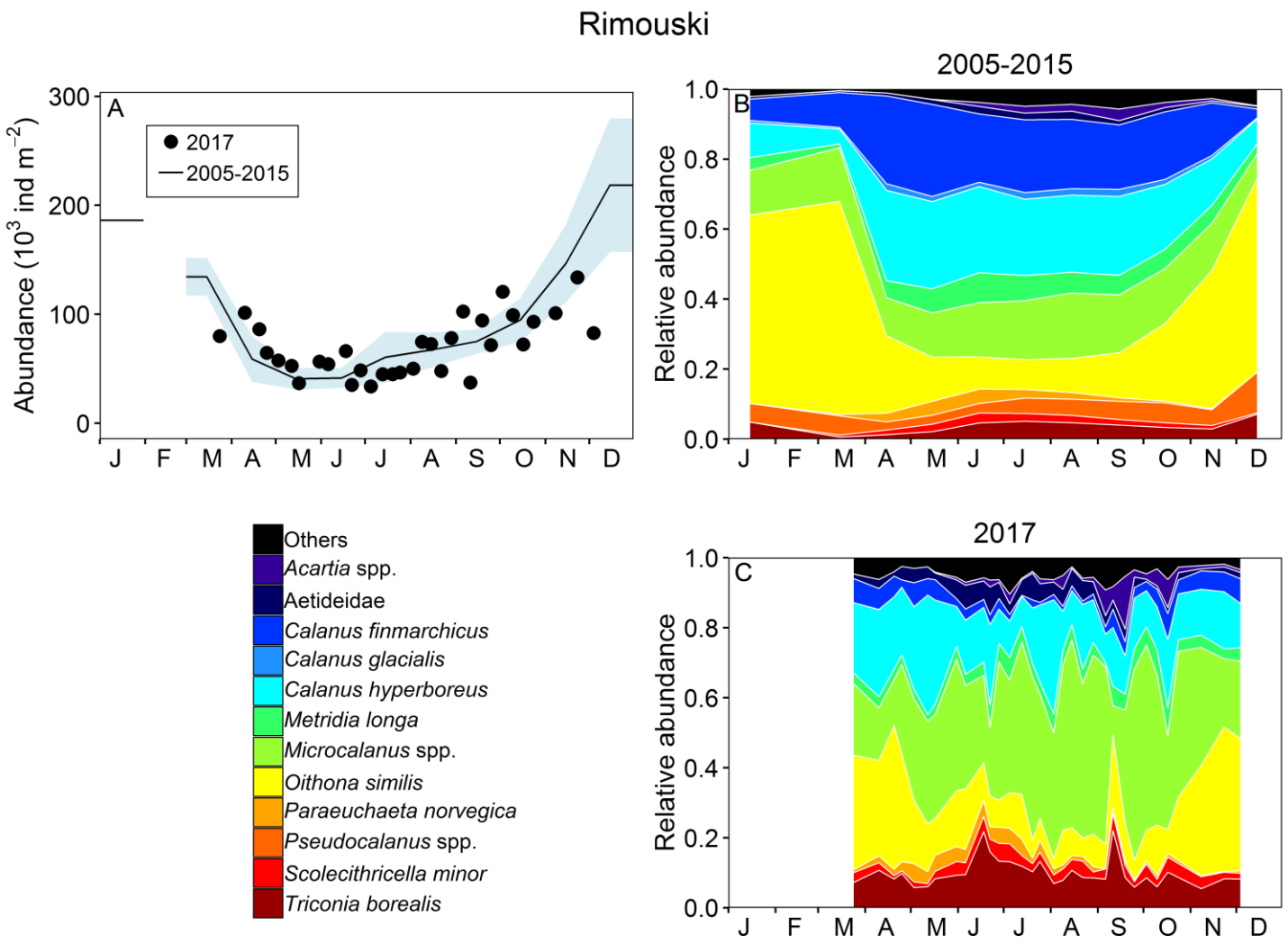

Figure 23. Seasonal variability of dominant copepods at Rimouski station. Copepod abundance (excluding nauplii) during the reference period (black line with blue shading indicating 0.5 SD) and in 2017 (circles) (A); climatology of the relative abundance of the top 95% of identified copepod taxa during the 2005–2015 period (B) and in 2017 (C).

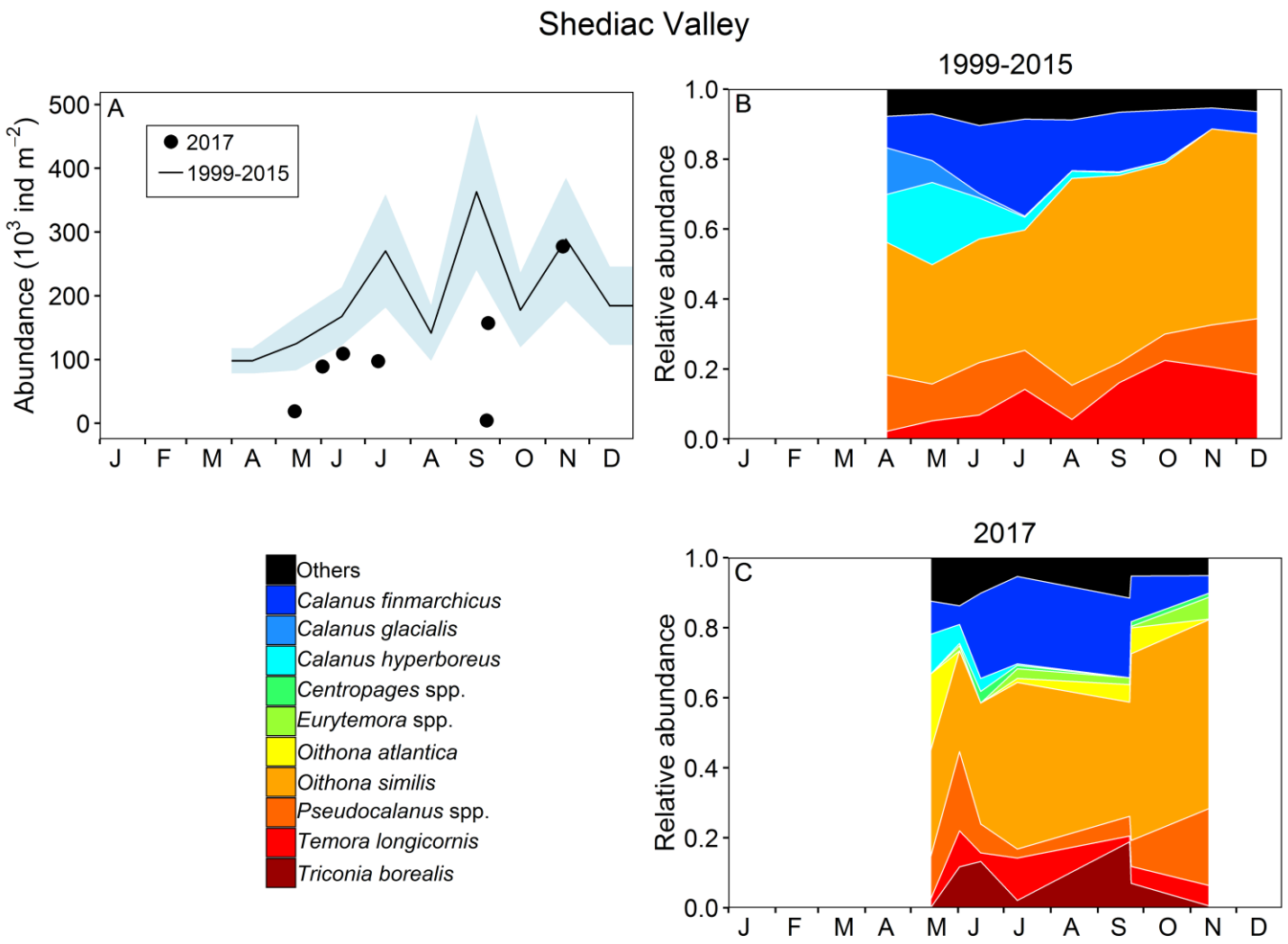

Figure 24. Seasonal variability of dominant copepods at Shediac Valley station. Copepod abundance (excluding nauplii) during the reference period (black line with blue shading indicating 0.5 SD) and 2017 (circles) (A); climatology of the relative abundance of the top 95% of identified copepod taxa during the 1999–2015 period (B) and in 2017 (C).

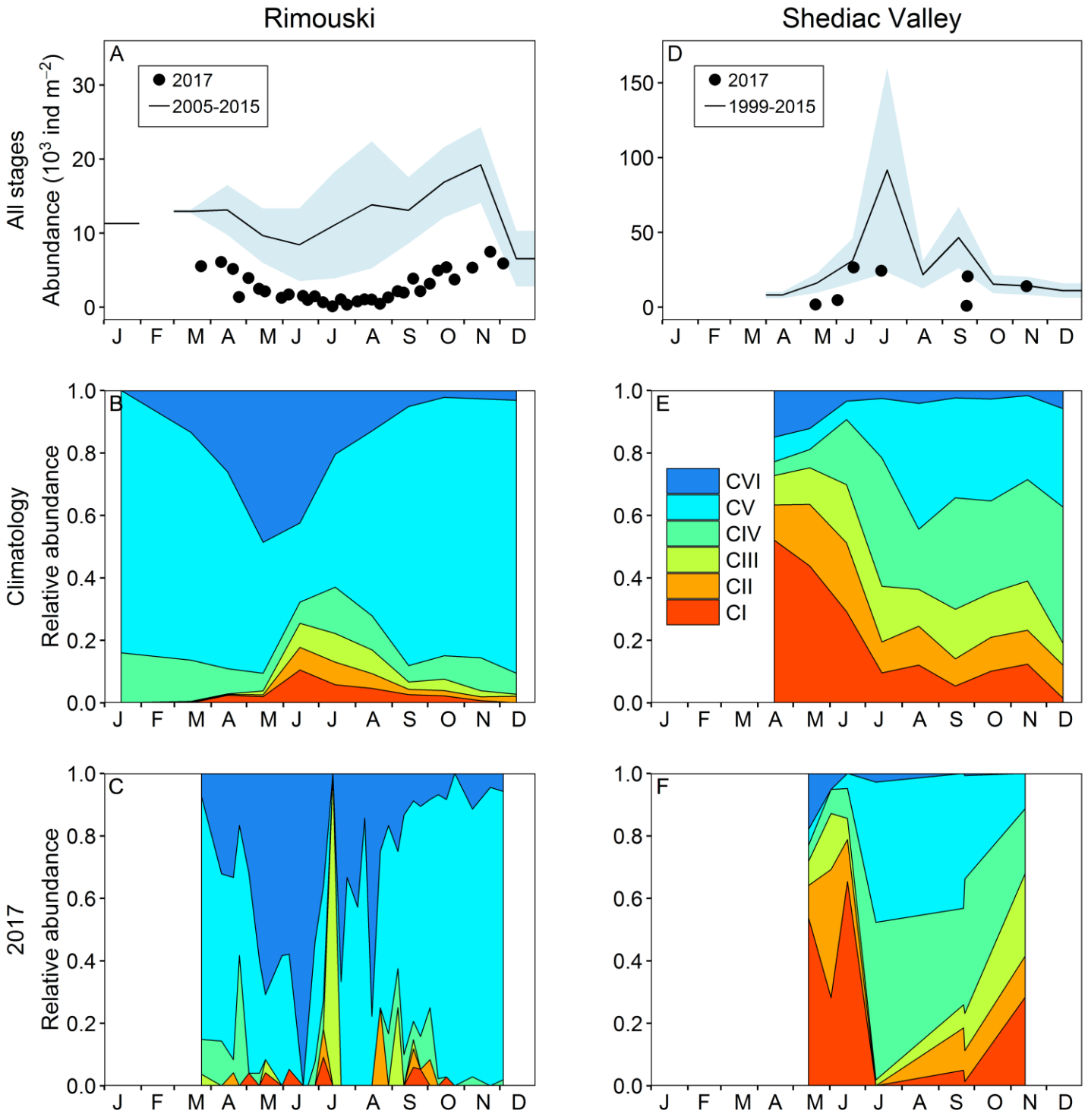

Figure 25. Seasonal variability in Calanus finmarchicus *copepodite abundance at Rimouski (A–C) and Shediac Valley (D–F) stations. The climatologies of the combined counts for the reference periods (black line with blue shading indicating 0.5 SD) are plotted with data from 2017 (circles) (A, D). The seasonal variabilities for the individual copepodite stages for the reference periods (B, E) and for 2017 (C, F) are also shown.*

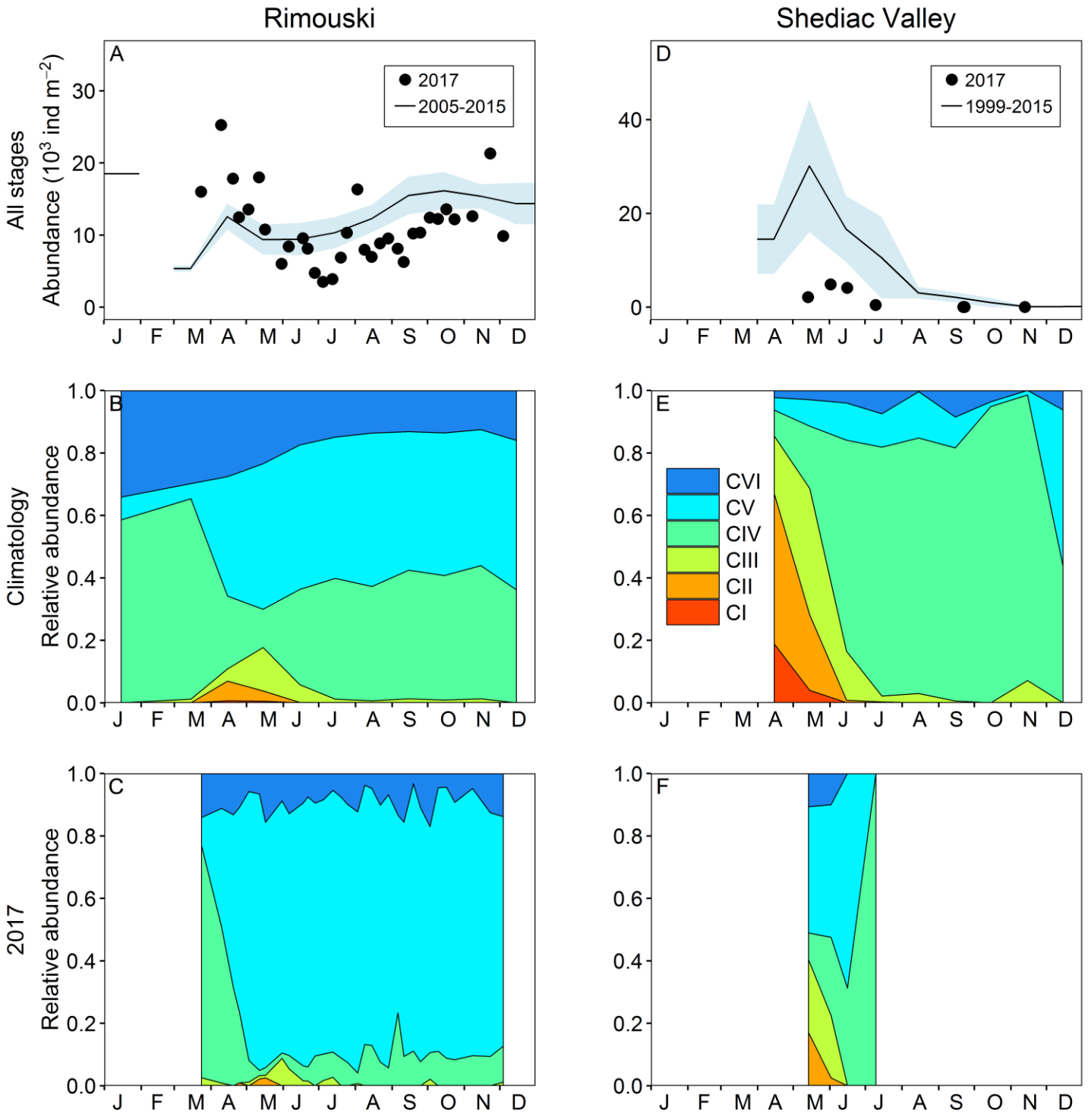

Figure 26. Seasonal variability in Calanus hyperboreus *copepodite abundance at Rimouski (A–C) and Shediac Valley (D–F) stations. The climatologies of the combined counts for the reference periods (black line with blue shading indicating 0.5 SD) are plotted with data from 2017 (circles) (A, D). The seasonal variabilities for the individual copepodite stages for the reference periods (B, E) and for 2017 (C, F) are also shown.*

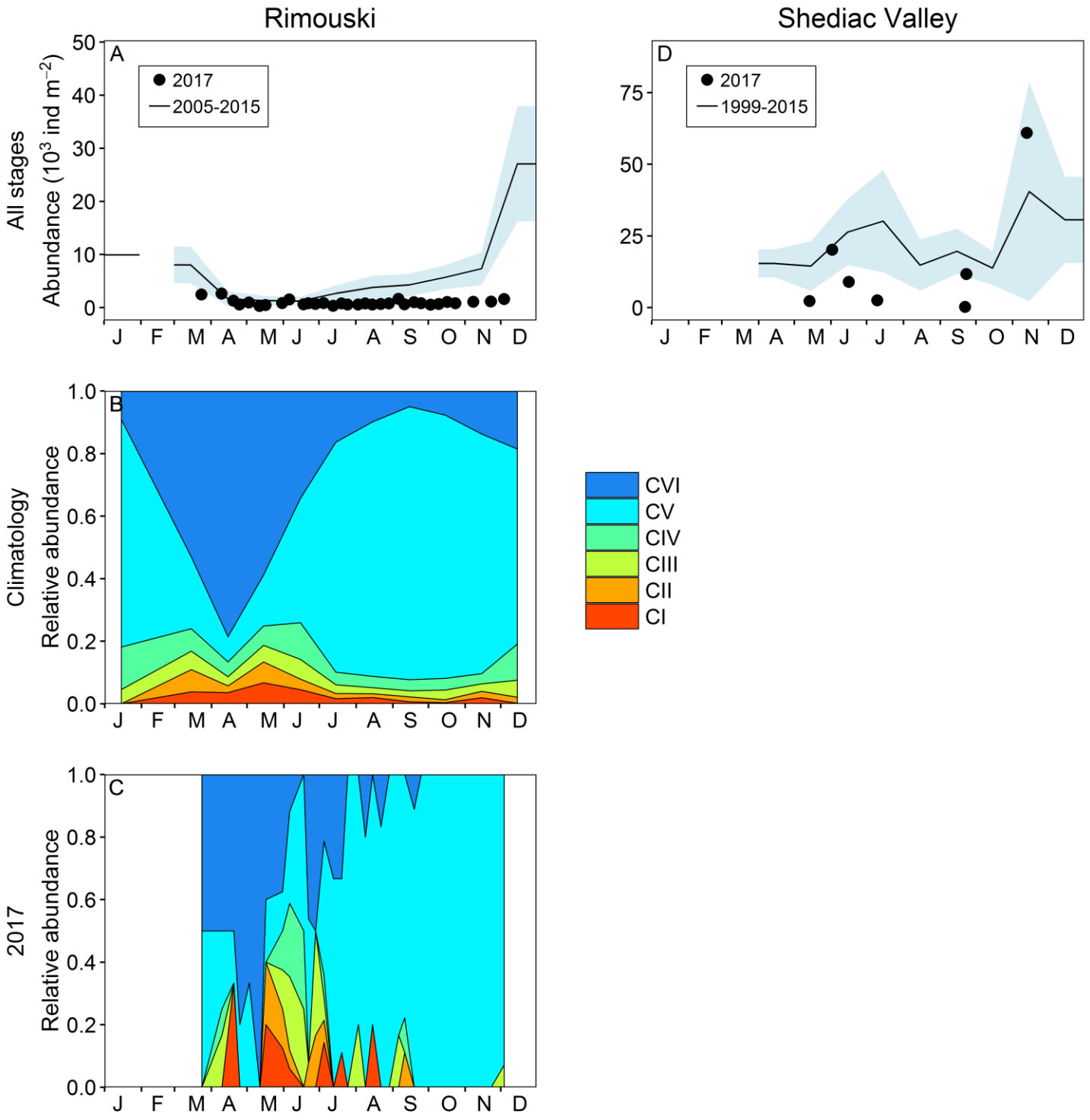

Figure 27. Seasonal variability in Pseudocalanus spp. copepodite abundance at Rimouski (A–C) and Shediac Valley (D) stations. The climatologies of the combined counts for the reference periods (black line with blue shading indicating 0.5 SD) are plotted with data from 2017 (circles) (A, D). Seasonal variability for the individual copepodite stages for the reference period (B) and for 2017 (C) are also shown. No stage information is available for Shediac Valley.

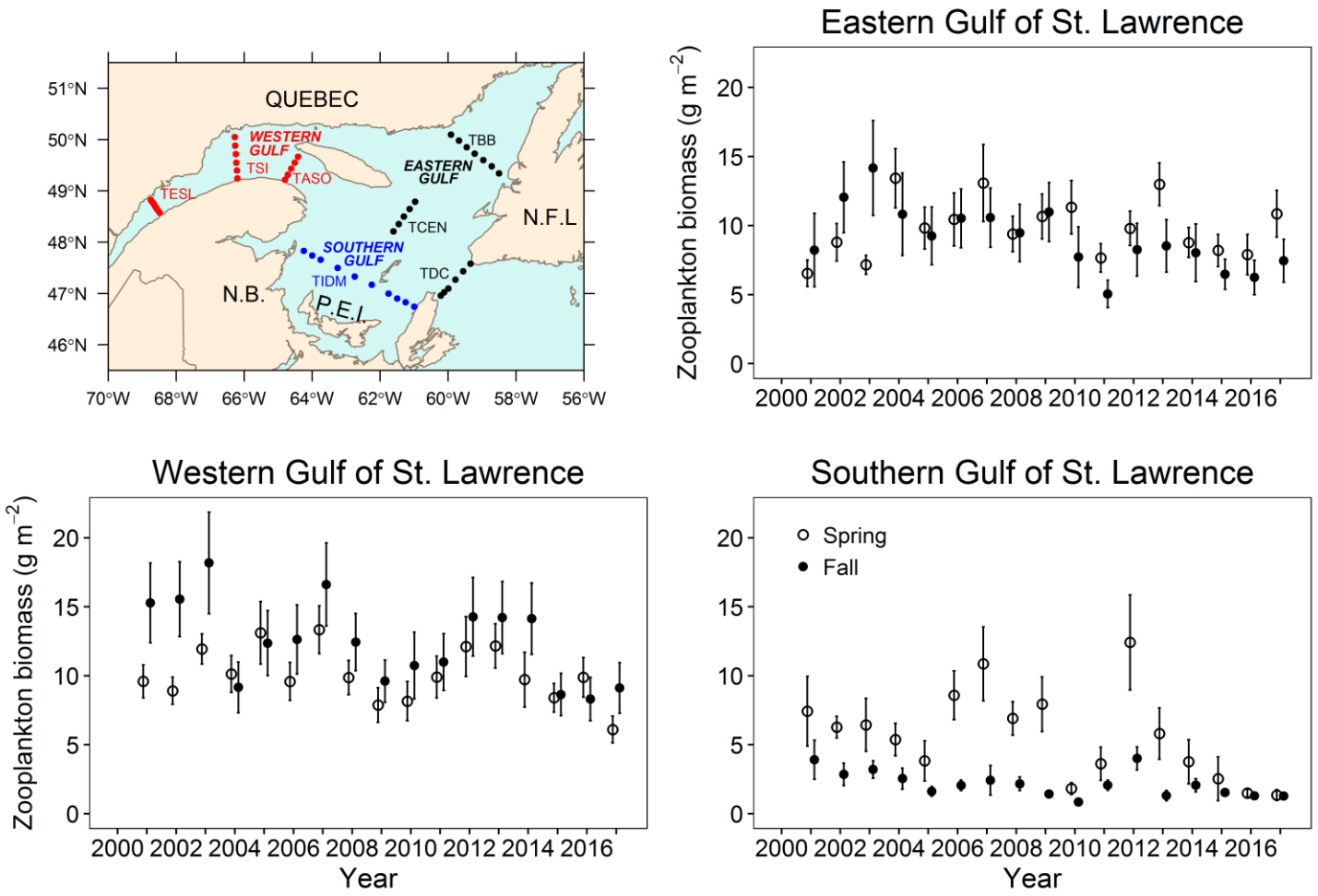

Figure 28. Time series of mean total zooplankton biomass (dry weight) during spring (open circles) and fall (filled circles) for the three subregions of the Gulf of St. Lawrence. Vertical lines represent standard errors.

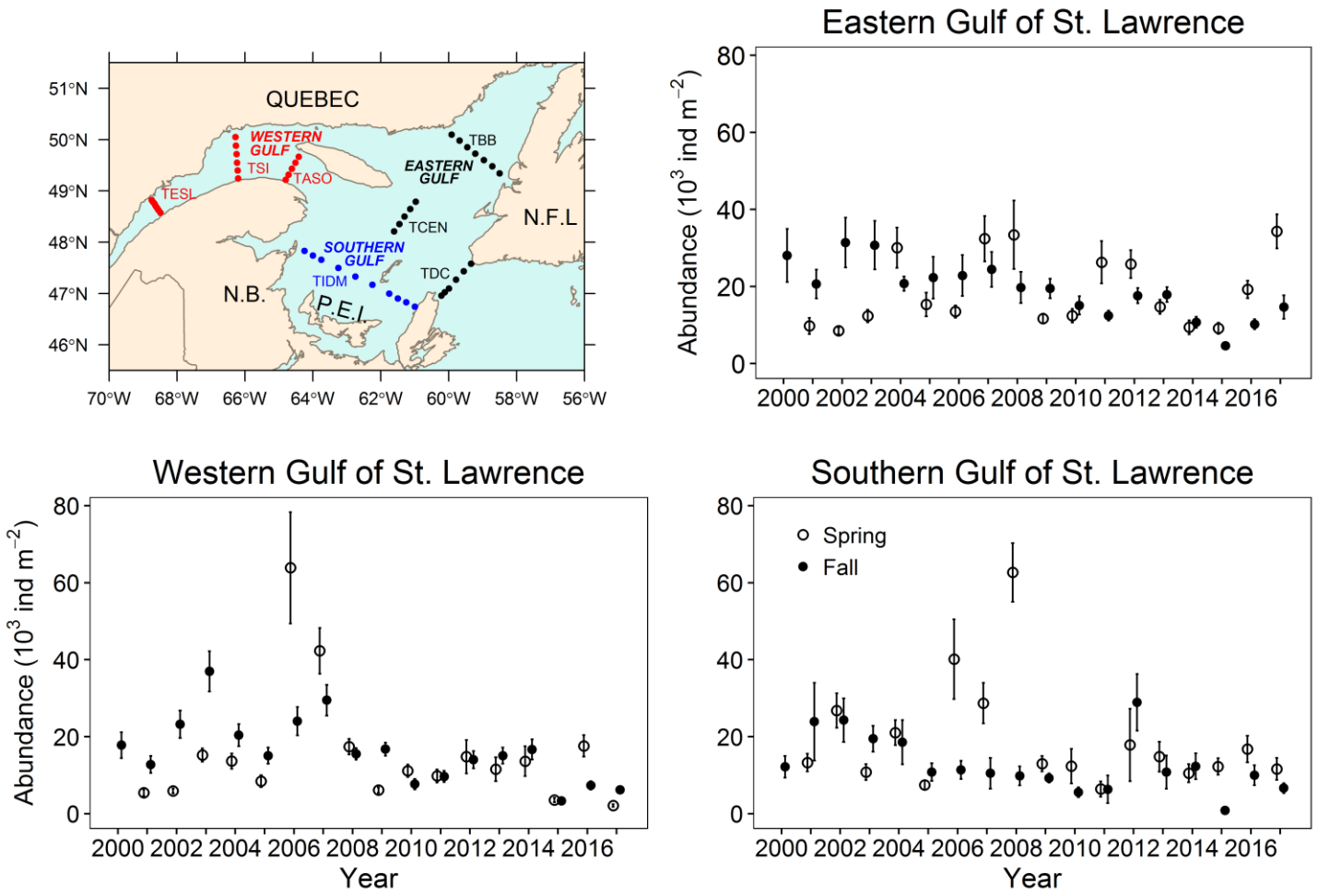

Figure 29. Time series of mean total abundance of Calanus finmarchicus *during spring (open circles) and fall (filled circles) for the three subregions of the Gulf of St. Lawrence. Vertical lines represent standard errors.*

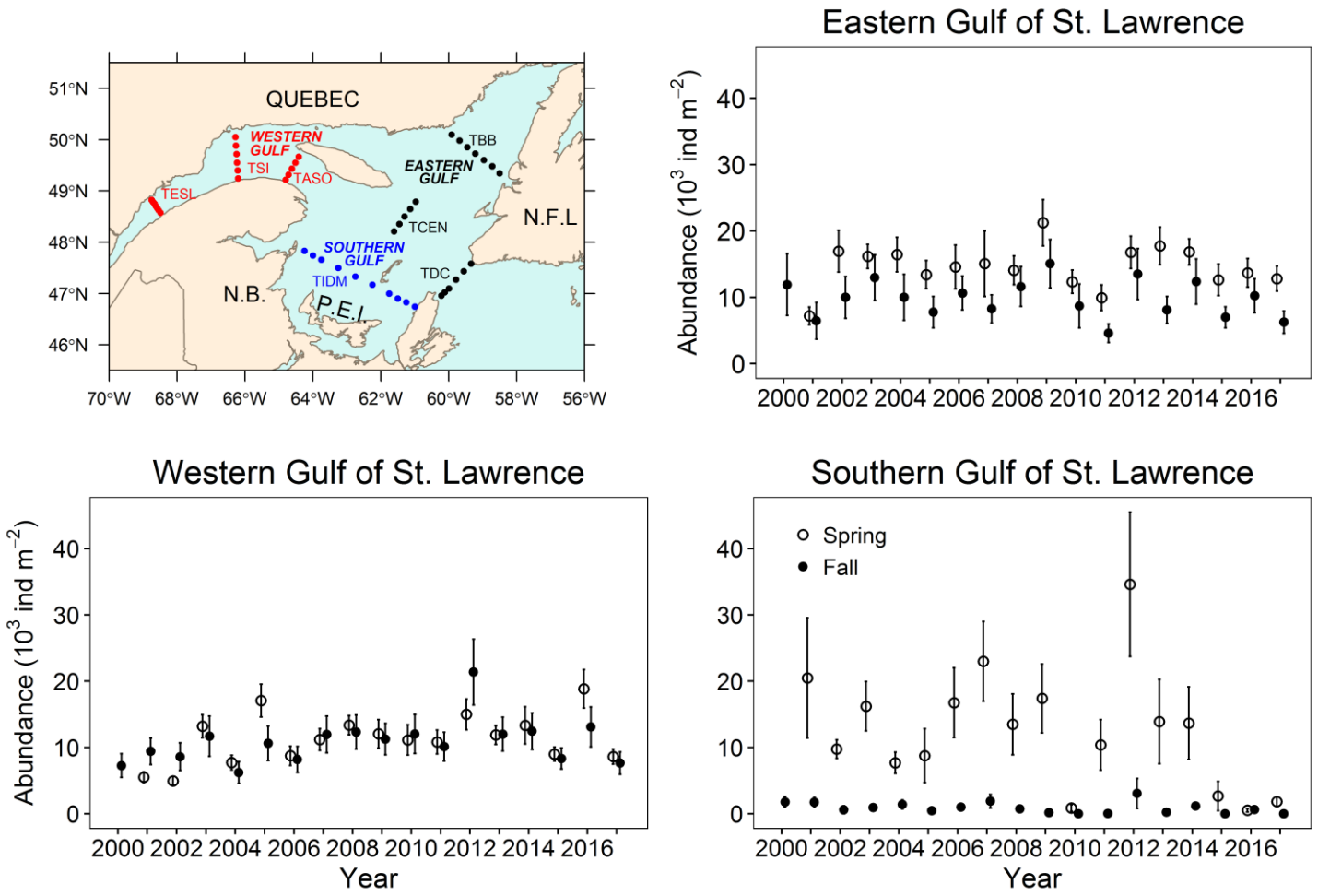

Figure 30. Time series of mean total abundance of Calanus hyperboreus *during spring (open circles) and fall (filled circles) for the three subregions of the Gulf of St. Lawrence. Vertical lines represent standard errors.*

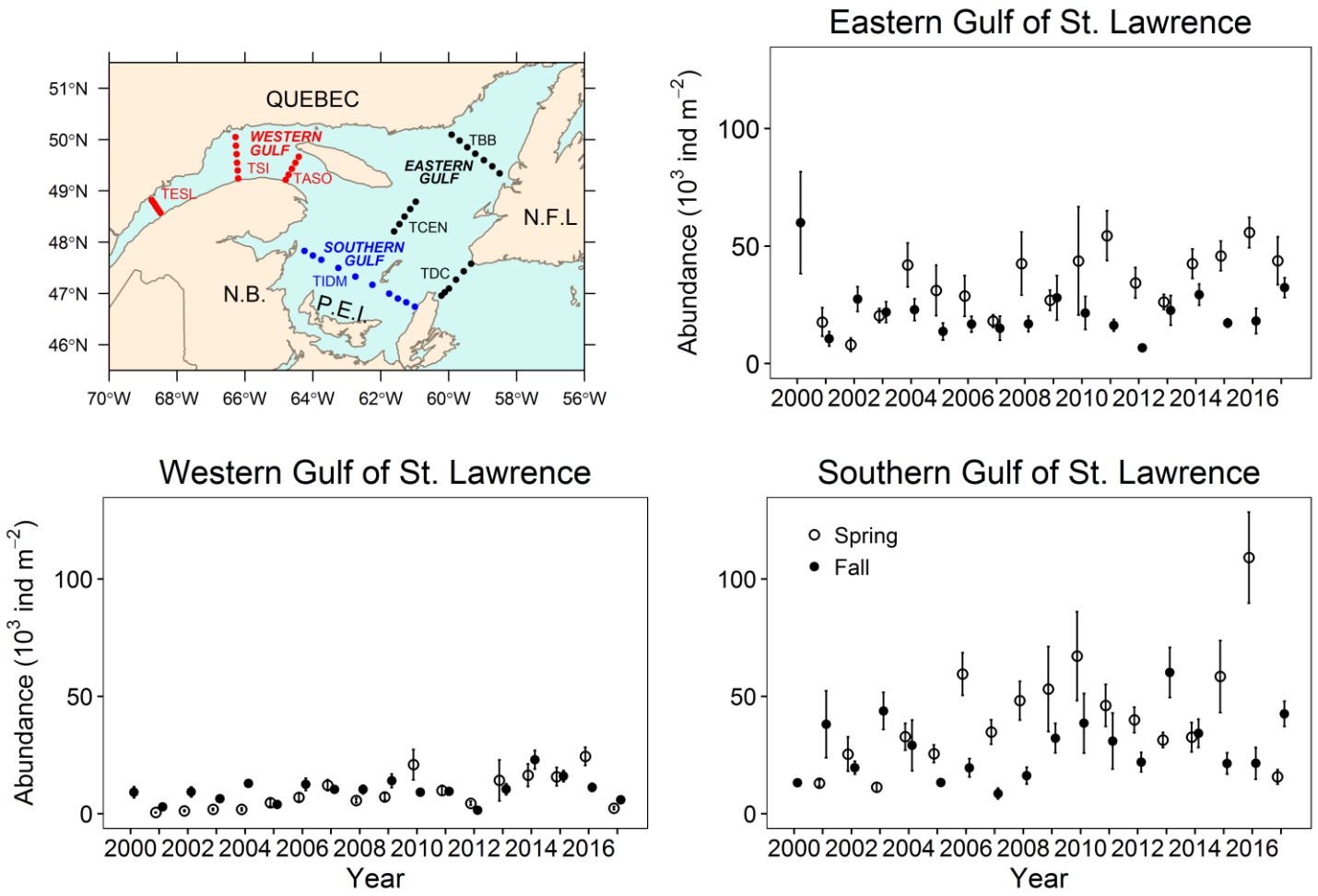

Figure 31. Time series of mean total abundance of Pseudocalanus *spp. during spring (open circles) and fall (filled circles) for the three subregions of the Gulf of St. Lawrence. Vertical lines represent standard errors.*

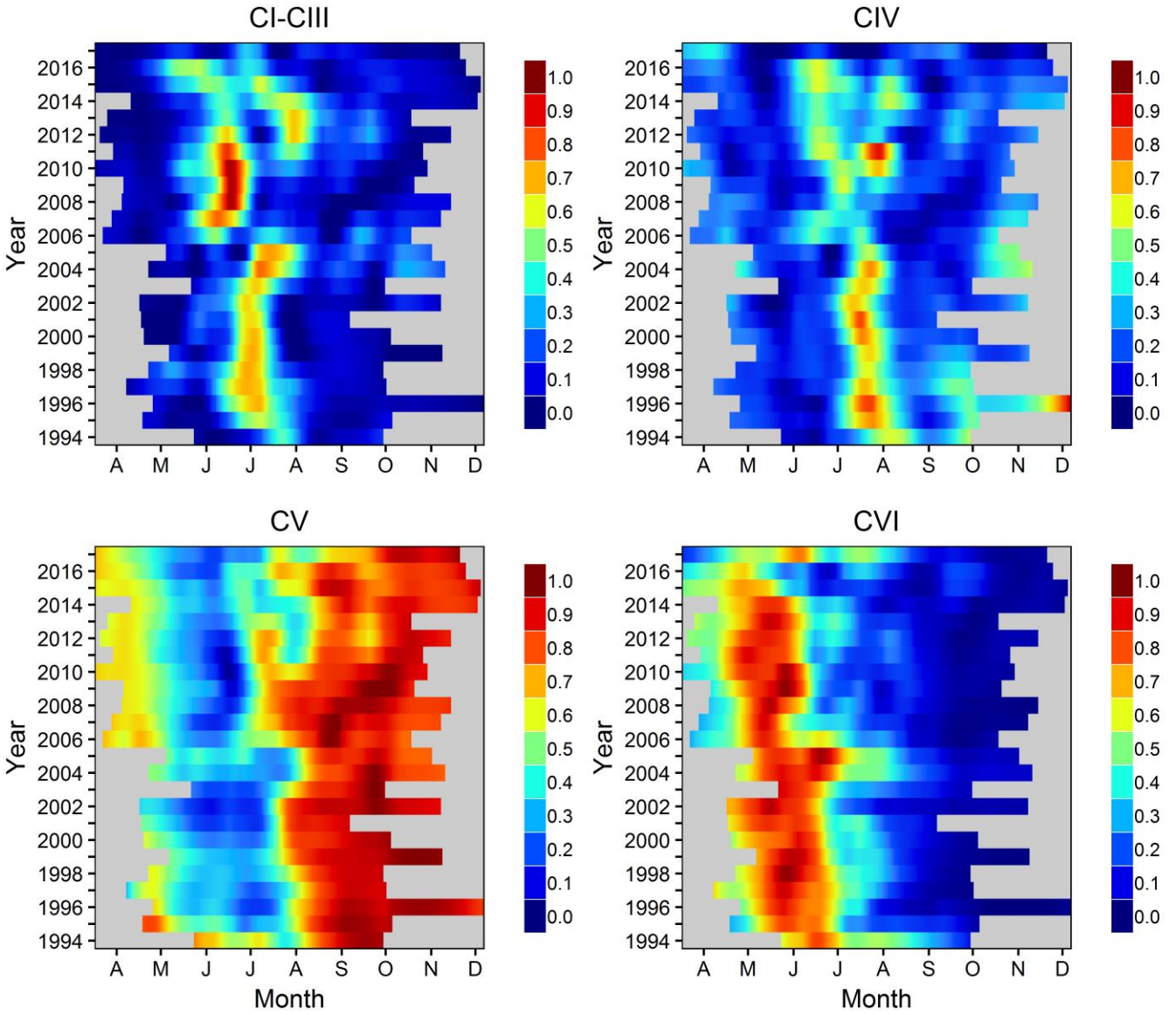

Figure 32. Time series of the seasonal cycle in relative proportions of total abundance for Calanus finmarchicus *copepodite stages (CI–CIII, CIV, CV, and CVI male + female) at Rimouski station. Proportions are normalized by the annual maximum and smoothed using a Loess.*

Biomass	1999	2000	2001	2002	2003	2004	2005	2006	2007	2008	2009	2010	2011	2012	2013	2014	2015	2016	2017	Mean	SD
Rimouski							0.13	0.24	1.48	1.13	-1.69	-1.58	0.26	-0.53	0.03	0.82	-0.29	-1.13	-1.30	12.7	2.8
wGSL			0.57	0.24	1.52	-0.67	-0.04	-0.15	1.64	-0.35	-1.49	-1.01	-0.51	0.99	0.93	-0.03	-1.64	-1.19	-1.97	11.4	1.9
eGSL			-0.26	1.50	0.58	1.56	-0.28	0.24	1.16	-0.34	0.43	-0.19	-2.03	-0.56	0.39	-0.91	-1.29	-1.50	-0.49	10.0	1.8
Shediac Valley	-1.35	0.75	0.83	-0.37	2.33	0.34	-0.93	0.83	0.18	-0.74	0.45	-1.33	-1.31	0.83	-0.14	0.38	-0.76	-1.41	-1.91	3.9	2.1
sGSL			0.73	0.14	0.32	-0.14	-0.73	0.61	1.31	0.19	0.27	-1.81	-0.71	2.15	-0.33	-0.76	-1.24	-1.48	-1.63	4.2	1.9

Figure 33. Time series of normalized annual anomalies for the zooplankton biomass (dry weight; g m^{-2}) at the high-frequency monitoring sites and the three subregions of the Gulf of St. Lawrence. Variable means and standard deviations for the1999–2015 (2005–2015 for Rimouski) reference period are shown at the right end of the scorecard. Blue colours indicate anomalies below the mean and reds are anomalies above the mean.

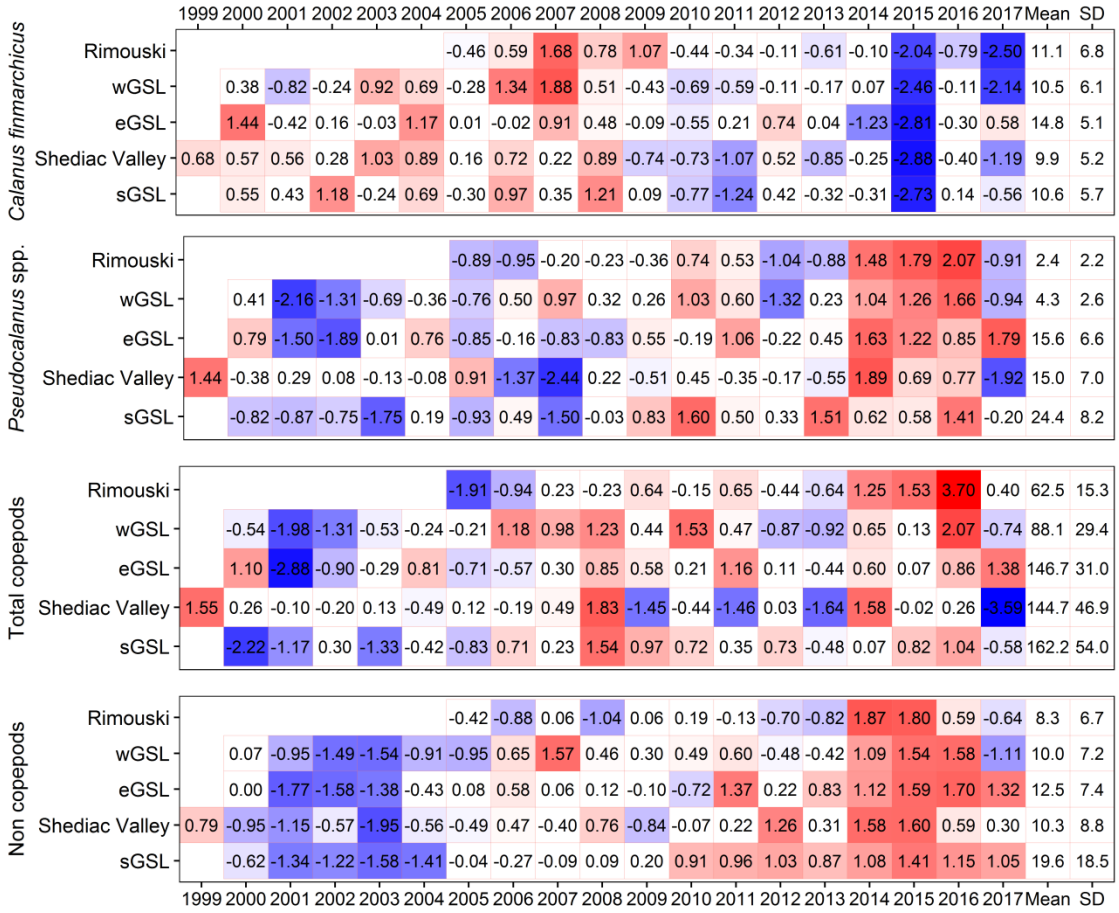

Figure 34. Time series of normalized annual anomalies for the abundance (×10^3 ind m^{-2}) of four zooplankton categories at the high-frequency monitoring sites and the three subregions of the Gulf of St. Lawrence. Variable means and standard deviations for the1999–2015 (2005–2015 for Rimouski) reference period are shown at the right end of the scorecard. Blue colours indicate anomalies below the mean and reds are anomalies above the mean.

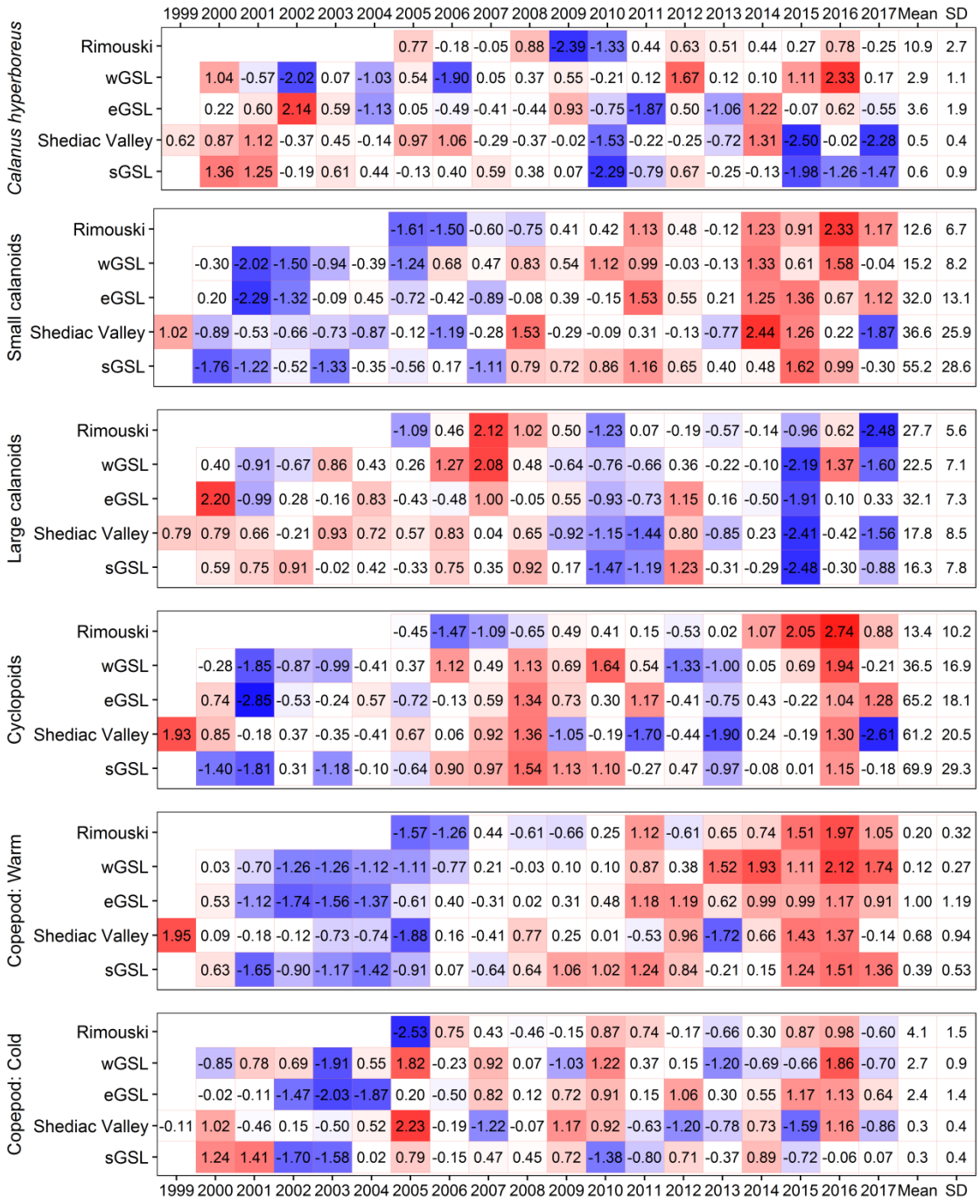

Figure 35. Time series of normalized annual anomalies for the abundance (×10^3 ind m^{-2}) of six categories of zooplankton assemblages at the high-frequency monitoring sites and the three subregions of the Gulf of St. Lawrence. Variable means and standard deviations for the1999–2015 (2005–2015 for Rimouski) reference period are shown at the right end of the scorecard. Blue colours indicate anomalies below the mean and reds are anomalies above the mean. Small calanoids: mostly neritic species such as Pseudocalanus spp., Acartia spp., Temora longicornis, and Centropages spp.; large calanoids: mostly Calanus and Metridia species; cyclopoids: mostly Oithona spp. and Triconia spp.; warm-water species: Metridia lucens, Centropages spp., Paracalanus spp., and Clausocalanus spp.; and cold/arctic species: Calanus glacialis and Metridia longa.

APPENDICES

Appendix 1. GLM results for Rimouski and Shediac Valley stations. Significance of the year and month effects as well as the adjusted R squared of the regression for each group are presented.

Region	Group	year (*p*)	month (*p*)	R^2
Rimouski	*Calanus finmarchicus*	<0.0001	<0.0001	0.55
	Pseudocalanus spp.	<0.0001	<0.0001	0.56
	Total copepods	<0.0001	<0.0001	0.56
	Non-copepods	<0.0001	<0.0001	0.44
	Calanus hyperboreus	<0.0001	<0.0001	0.38
	Small calanoids	<0.0001	<0.0001	0.65
	Large calanoids	<0.0001	<0.0001	0.3
	Cyclopoids	<0.0001	<0.0001	0.58
	Copepods: Warm	<0.0001	0.9	0.54
	Copepods: Cold	<0.0001	<0.0001	0.44
Shediac Valley	*Calanus finmarchicus*	<0.0001	<0.0001	0.34
	Pseudocalanus spp.	0.2	0.2	0.03
	Total copepods	0.1	<0.0001	0.18
	Non-copepods	0.001	0.0003	0.24
	Calanus hyperboreus	<0.0001	<0.0001	0.66
	Small calanoids	0.01	0.0003	0.18
	Large calanoids	<0.0001	<0.0001	0.37
	Cyclopoids	0.2	<0.0001	0.24
	Copepods: Warm	0.1	0.06	0.08
	Copepods: Cold	0.2	<0.0001	0.29

Appendix 2. GLM results for GSL subregions. Significance of the year, season, and station effects as well as the adjusted R squared of the regression for each group are presented.

Region	Group	year (*p*)	season (*p*)	station(*p*)	R^2
wGSL	*Calanus finmarchicus*	<0.0001	0.001	<0.0001	0.68
	Pseudocalanus spp.	<0.0001	<0.0001	<0.0001	0.53
	Total copepods	<0.0001	<0.0001	<0.0001	0.76
	Non-copepods	<0.0001	<0.0001	<0.0001	0.60
	Calanus hyperboreus	0.003	<0.0001	<0.0001	0.61
	Small calanoids	<0.0001	<0.0001	<0.0001	0.68
	Large calanoids	<0.0001	0.02	<0.0001	0.78
	Cyclopoids	<0.0001	<0.0001	<0.0001	0.71
	Copepods: Warm	<0.0001	0.05	<0.0001	0.52
	Copepods: Cold	<0.0001	<0.0001	<0.0001	0.66
sGSL	*Calanus finmarchicus*	<0.0001	<0.0001	<0.0001	0.31
	Pseudocalanus spp.	<0.0001	<0.0001	0.8	0.13
	Total copepods	<0.0001	<0.0001	0.0005	0.32
	Non copepods	<0.0001	<0.0001	<0.0001	0.53
	Calanus hyperboreus	<0.0001	<0.0001	<0.0001	0.49
	Small calanoids	<0.0001	0.003	0.01	0.28
	Large calanoids	<0.0001	<0.0001	<0.0001	0.48
	Cyclopoids	<0.0001	<0.0001	<0.0001	0.37
	Copepods: Warm	<0.0001	<0.0001	0.3	0.52
	Copepods: Cold	<0.0001	<0.0001	<0.0001	0.40
eGSL	*Calanus finmarchicus*	<0.0001	0.3	<0.0001	0.22
	Pseudocalanus spp.	<0.0001	<0.0001	<0.0001	0.27
	Total copepods	<0.0001	<0.0001	<0.0001	0.27
	Non-copepods	<0.0001	<0.0001	<0.0001	0.45
	Calanus hyperboreus	0.1	<0.0001	<0.0001	0.54
	Small calanoids	<0.0001	0.9	<0.0001	0.37
	Large calanoids	<0.0001	<0.0001	<0.0001	0.48
	Cyclopoids	<0.0001	<0.0001	0.002	0.32
	Copepods: Warm	<0.0001	<0.0001	<0.0001	0.50
	Copepods: Cold	<0.0001	<0.0001	<0.0001	0.38